Prerequisites for Explosive Cryovolcanism on Dwarf Planet-Class Kuiper Belt Objects

M. Neveu[a,*], S. J. Desch[a], E. L. Shock[a,b], C. R. Glein[c]

[a] *School of Earth and Space Exploration, Arizona State University, Tempe, AZ 85287-1404, USA*
[b] *Department of Chemistry and Biochemistry, Arizona State University, Tempe, AZ 85287-1404, USA*
[c] *Geophysical Laboratory, Carnegie Institution of Washington, 5251 Broad Branch Rd. NW, Washington, DC 20015, USA*

Abstract

Explosive extrusion of cold material from the interior of icy bodies, or cryovolcanism, has been observed on Enceladus and, perhaps, Europa, Triton, and Ceres. It may explain the observed evidence for a young surface on Charon (Pluto's surface is masked by frosts). Here, we evaluate prerequisites for cryovolcanism on dwarf planet-class Kuiper belt objects (KBOs). We first review the likely spatial and temporal extent of subsurface liquid, proposed mechanisms to overcome the negative buoyancy of liquid water in ice, and the volatile inventory of KBOs. We then present a new geochemical equilibrium model for volatile exsolution and its ability to drive upward crack propagation. This novel approach bridges geophysics and geochemistry, and extends geochemical modeling to the seldom-explored realm of liquid water at subzero temperatures. We show that carbon monoxide (CO) is a key volatile for gas-driven fluid ascent; whereas CO_2 and sulfur gases only play a minor role. N_2, CH_4, and H_2 exsolution may also drive explosive cryovolcanism if hydrothermal activity produces these species in large amounts (a few percent with respect to water). Another important control on crack propagation is the internal structure: a hydrated core makes explosive cryovolcanism easier, but an undifferentiated crust does not. We briefly discuss other controls on ascent such as fluid freezing on crack walls, and outline theoretical advances necessary to better understand cryovolcanic processes. Finally, we make testable predictions for the 2015 *New Horizons* flyby of the Pluto-Charon system.

Keywords:
Charon, Interiors, Pluto, satellites, formation, volcanism

1. Introduction

Cryovolcanism is *"the eruption of liquid or vapor phases (with or without entrained solids) of water or other volatiles that would be frozen solid at the normal temperature of the icy satellites surface"* (Geissler, 2000). It is a clear marker of extant geological activity, and planetary bodies that show evidence for or suggestive of cryovolcanism, such as Europa, Titan, Enceladus, and Triton are the foci of many planetary science and astrobiology investigations. Cryovolcanism could occur by either effusive or explosive processes (e.g. Fagents, 2003). Evidence for past or recent effusive activity has remained inconclusive, because of the difficulty to distinguish cryovolcanic from diapiric surface morphologies (Fagents, 2003; Lopes et al., 2007). Gas-driven activity, on the other hand, has been unmistakably identified in the form of plumes on Triton, Enceladus, and perhaps Europa and Ceres (Kirk et al., 1995; Porco et al., 2006; Roth et al., 2014; Küppers et al., 2014). The upcoming flyby of the Pluto-Charon system by the *New Horizons* spacecraft brings a new opportunity to look for plumes on Pluto and Charon that would imply extensive geophysical and geochemical activity on these icy dwarf planets. The scope of this paper is to evaluate the likelihood of extant cryovolcanism on dwarf planet-class Kuiper belt objects (KBOs) from our current knowledge of explosive cryovolcanic processes, the volatile inventory in the Kuiper belt, and the thermal evolution of KBOs. To this end, we use a novel approach that couples geophysics and geochemistry, and extends predictive geochemical modeling to the domain of liquid water at subzero temperatures. We begin in this introduction by briefly reviewing evidence for explosive cryovolcanism in the outer solar system. In the following section, we review previous theoretical results on gas-driven cryovolcanism, as well as current knowledge of the volatile inventory of KBOs. Building on these results, we then present a new geochemical model for gas exsolution to drive the propagation of fluid-filled cracks to the surface. Next, we discuss other controls on fluid ascent, such as the presence of a primordial ice-rock crust or fluid freezing in the cracks. We conclude by making predictions on the possibility of cryovolcanism on Pluto, Charon, and KBOs of similar size.

1.1. Explosive volcanism and outgassing

Outgassing of volatiles by a planetary body may occur by sublimation of ices close to the surface, as this surface is heated by a source external to the body, such as the Sun or an impact. Alternatively, the volatiles may originate much deeper inside the body, and the cause of their outgassing be rooted in endogenic heating processes. Here, we call the former phenomenon

*Corresponding author
Email address: MNeveu@asu.edu (M. Neveu)

"sublimation" and the latter "explosive cryovolcanism", and we use "outgassing" as a generic term. These processes can all result in observable plumes, and only more detailed analyses (e.g. of their chemical composition or thermal emission) can conclusively determine the cause of outgassing.

For KBOs, the semantics are complicated because two communities have investigated their origins, evolution, and present state. The "large icy satellites" community sees KBOs as mini-worlds with possible geophysical evolution over geological timescales; their viewpoint applies to bodies large enough to be differentiated, with little porosity, and which may have sustained subsurface liquid water. Such bodies may have enough endogenic energy to drive explosive cryovolcanism as understood in the viewpoint of icy satellites (Crawford and Stevenson, 1988; Fagents, 2003; Hansen et al., 2006), although sublimation may also occur. On the other hand, the "small primitive bodies" community sees the Kuiper belt as a reservoir of comet nuclei that have undergone little or no evolution since their formation; their viewpoint applies to smaller (<100 km), undifferentiated bodies, with significant porosity, and no liquid. For these bodies, as for comets, surface manifestations of outgassing are necessarily due to sublimation, except perhaps early in their history (De Sanctis et al., 2001; Choi et al., 2002). Here, we focus on KBOs for which the "large icy satellite" viewpoint applies. These may be referred to as dwarf planet-class KBOs; we call them KBOs for short in the rest of this paper.

1.2. Evidence for cryovolcanism in the outer solar system

Extant outgassing has been so far conclusively observed in the form of N_2 gas plumes on Triton, assumed to be a KBO captured by Neptune (Smith et al., 1989; Soderblom et al., 1990; Kirk et al., 1995) and H_2O plumes on Enceladus (Hansen et al., 2006; Porco et al., 2006; Matson et al., 2007; Postberg et al., 2009; Waite Jr et al., 2009). An observation of plumes on Europa has also been recently reported (Roth et al., 2014), as well as water emission from Ceres localized in space and time (Küppers et al., 2014). For Triton, although both exogenic and endogenic sources have been suggested to drive the N_2 eruptions, the N_2 may originate in a layer close to the surface (Brown et al., 1990; Ingersoll and Tryka, 1990), but may nonetheless reveal a regime of convection in Triton's icy mantle (Duxbury and Brown, 1997). Triton also experienced an early phase of heating by tidal dissipation during its capture by Neptune (Shock and McKinnon, 1993). On Enceladus, the cryovolcanic interpretation is favored because the plume ejects species such as NaCl and silica; this suggests that the source of the plume contains material leached from Enceladus' rocky core (Postberg et al., 2009, Hsu et al., in preparation, Sekine et al., in preparation). Moreover, the plume activity is synchronized to Enceladus' orbit, with a surge when Enceladus is farthest from Saturn such that South Pole fractures experience tensile tidal stresses (Hedman et al., 2013). *Cassini* observations of Titan suggest that it too is undergoing cryovolcanism, although this remains uncertain (Sotin et al., 2005; Nelson et al., 2009); cryovolcanism could explain the presence of argon-40 and methane in Titan's atmosphere (Tobie et al., 2006). Recently, ground-based observations of an aurora near the south pole of Europa have strongly suggested that it too is experiencing explosive cryovolcanism (Roth et al., 2014). As for Enceladus, plume activity occurs when Europa is farthest from Jupiter, and seems to depend on tidal stresses (Roth et al., 2014). The radii (250 to 2575 km) and densities of these moons (1.6 to 3.0 g cm^{-3}) bracket those of the Kuiper Belt Objects (KBOs) Pluto and Charon [1150 and 600 km; 2.0 and 1.6 g cm^3; Buie et al. (2006)]. This suggests bulk compositions, internal structures, and thermal histories similar to those of the icy satellites, with the notable exception that Pluto and Charon may have experienced little or no tidal heating.

Several observations of KBO surfaces are suggestive of recent cryovolcanic eruptions, whether effusive or explosive. First, short-lived ammonia hydrates have been detected on the surfaces of Charon and, likely, Orcus (Brown and Calvin, 2000; Cook et al., 2007; Merlin et al., 2010; Delsanti et al., 2010). These compounds should be destroyed by solar ultraviolet radiation and galactic cosmic rays on timescales shorter than 1 to 50 Myr (Jewitt and Luu, 2004; Cook et al., 2007), and no mechanism other than recent localized resurfacing by cryovolcanism has conclusively explained their presence on Charon's surface (Jewitt and Luu, 2004; Cook et al., 2007; McKinnon et al., 2008; Desch et al., 2009; Brown, 2012). The presence of abundant crystalline ice has also been suggested as evidence for resurfacing, because it too should be amorphized on short timescales; however, its presence on KBOs much too small to be geologically active (Brown, 2012) suggests that another process must be at play, such as annealing of amorphous ice by dust impacts (Porter et al., 2010). More generally, cryovolcanism has been invoked to explain the observation of volatile ices other than water (mainly N_2, CH_4, CH_3OH, and NH_3) on KBO surfaces [see recent reviews by McKinnon et al. (2008) and Brown (2012)].

Evidence and mechanisms for effusive volcanism have previously been investigated. For example, Fagents (2003) reviewed a dozen studies that proposed past effusive cryovolcanism to explain morphologies on satellites of Jupiter (Europa and Ganymede), Saturn (Enceladus, Dione, Tethys, and Iapetus), and Uranus (Miranda and Ariel). These morphologies include *"smooth and/or sparsely cratered surfaces, infilled craters and graben, domes, lobate features, ridges, caldera-like features, and low-albedo surfaces"* (Fagents, 2003). Recently, similar morphologies have been studied on Titan using *Cassini* radar and infrared imagery (Lopes et al., 2007; Wall et al., 2009; Le Corre et al., 2009; Soderblom et al., 2009). To assess the possible cryovolcanic origin of these observed morphologies, laboratory experiments and modeling studies have investigated the rheological properties of cryolavas of water-volatile compositions (Schenk, 1991; Kargel et al., 1991; Zhong et al., 2009). Similar effusive morphologies may certainly also occur on KBOs and may well be observed by *New Horizons* at Pluto and Charon. However, as for the icy satellites, it is unlikely that a clear distinction between a cryovolcanic versus diapiric origin of such features will be made. Therefore, for the remainder of this paper, we focus exclusively on predicting the likelihood of *explosive* cryovolcanism on KBOs, which results in outgassing plumes that should be unambiguously detected by

New Horizons if presently occurring on Pluto or Charon.

2. Ingredients for explosive cryovolcanism

2.1. Liquid persistence

Extant explosive cryovolcanism requires the persistence of fluid to the present day, either as a subsurface ocean layer, as a localized pocket of liquid in the icy mantle (Fagents, 2003; Schmidt et al., 2011), or as volatile molecules trapped in clathrate hydrates which may outgas upon heating. Liquid persistence depends strongly on body size and melting point depression by antifreezes (McKinnon et al., 2008; Desch et al., 2009).

Larger bodies have a lower surface area:volume ratio, which scales as the inverse of the radius of the body. Because radiogenic heat production scales with volume and heat transport fluxes scale with surface area, larger bodies evacuate heat less effectively. Therefore, their internal temperatures are higher and they are better able to maintain liquid.

Antifreezes are dissolved volatile or salt impurities that prevent water molecules from getting organized in a solid phase. Volatile antifreezes of relevance to icy bodies are ammonia NH_3 and methanol CH_3OH, two abundant compounds in comets (Mumma and Charnley, 2011, and references therein) that were likely accreted by Kuiper belt objects. The eutectic point of a water-ammonia mixture at 1 bar is depressed to about 176 K (Croft et al., 1988) and that of a water-methanol mixture is about 157 K (Miller and Carpenter, 1964). Relevant salt antifreezes are chlorides, carbonates, and especially sulfates (Kargel, 1991). These salts are components of chondrites (Kargel, 1991), the primitive rocky material likely accreted by KBOs, but they could also be leached from interactions between rock and liquid water.

The persistence of a liquid water layer for several Gyr, possibly to the present day, is a common outcome of geophysical evolution models of Pluto (Robuchon and Nimmo, 2011), Charon (Desch et al., 2009), and KBOs of similar dwarf-planet size. Pluto-sized bodies are more likely to retain liquid (even pure water at 273 K) in the absence of heat transfer by solid-state convection in the overlying ice shell, which transports heat outward more effectively than conduction (Robuchon and Nimmo, 2011). Smaller, Charon-sized bodies retain a liquid layer only if water contains dissolved antifreezes, or if an insulating undifferentiated crust mitigates heat loss over geologic time (Desch et al., 2009). Undifferentiated ice-rock crusts are insulating because the thermal conductivity of hydrated or chondritic rock, 0.5 to 2.5 W m^{-1} K^{-1} (Yomogida and Matsui, 1983; Clauser and Huenges, 1995; Opeil et al., 2010) is much lower than that of crystalline ice, 5.67 (100 K / T) W m^{-1} K^{-1} (Klinger, 1980). Such crusts are unstable gravitationally, but should not overturn over the age of the solar system due to the frigid temperatures and resulting high viscosity of ice near the surface of KBOs (Rubin et al., in review).

Therefore, the existence of subsurface liquid in KBOs for most of the age of the solar system, and possibly until the present day, is well motivated. If (a) heat transfer through ice shells is conductive rather than convective, (b) antifreezes are concentrated in water, and (c) Charon-sized KBOs retained crusts, the total amount of liquid water retained collectively by KBOs today may equal that of Earth's oceans (Desch et al., 2009).

2.2. Bringing cryolavas to the surface

2.2.1. Pressurization and crack opening

Cryovolcanism requires liquid to be lifted to the surface by overpressurization. This can be accomplished by freezing a small volume of water, raising the pressure in the remaining liquid. Freezing occurs because Pluto and Charon-sized KBOs cool after about 2 Gyr, when energy becomes transported to the surface and radiated to space faster than it is generated by long-lived radionuclides in the core (Desch et al., 2009; Robuchon and Nimmo, 2011). The overpressure ΔP generated by freezing a volume of liquid water is given by (Fagents, 2003):

$$\Delta P = \frac{f}{\beta_w (1-f)} \left(\frac{\rho_w}{\rho_i} - 1 \right) \quad (1)$$

where $\beta_w = -(1/V)(\partial V/\partial P)_T$ is the isothermal compressibility of water and f the fraction of water that freezes. This phenomenon causes the ice spikes one can sometimes see in ice cube trays in kitchen freezers. A large fluid-ice density contrast yields a higher overpressure, which is highest for pure liquid water freezing as pure ice, but becomes negligible for a eutectic mixture of H_2O-NH_3 freezing to ammonia dihydrate ice of similar density (Desch et al., 2009).

Equation (1) assumes a fixed volume of water. In reality, water exerts pressure on the walls of its container. In a global sense, water can raise the height of the ice shell. In a local sense, ice on the pocket walls can be compressed. Ice Ih at low pressure has a compressibility $\beta_i = 1.3 \times 10^{-10}$ Pa^{-1}, not too different from that of liquid water ($\beta_w = 5 \times 10^{-10}$ Pa^{-1}). Therefore, ice will also move or be compressed to some extent to accommodate the volume change due to freezing, and the overpressure in liquid water will not be quite as high as given by equation (1).

Regardless of this caveat, pressurization due to freezing is potent. Freezing just 1% of the ice overpressurizes a water pocket by $\Delta P = 2.0 \times 10^6$ Pa. At the top of a liquid water pocket, the overpressure (above the pressure of surrounding ice) is:

$$dP = \Delta P - (\rho_w - \rho_i) g (h - z) \quad (2)$$

where g is the gravitational acceleration (assumed constant), z the depth of the top of the pocket, and h the depth of the base of the pocket. Even for at the surface ($z = 0$), the overpressure is $dP = \Delta P - (\rho_w - \rho_i) g h = 2.0 \times 10^6$ Pa $- 1.2 \times 10^6$ Pa $= 0.8 \times 10^6$ Pa. This aids in the opening of cracks.

2.2.2. Crack propagation

Once a crack is open, can it keep propagating? Crawford and Stevenson (1988) investigated analytically a possible propagation mechanism using linear elastic fracture mechanics theory. If the normal stress intensity K_I in Pa $m^{1/2}$ exceeds a critical value K_{Ic}, the fracture toughness of the material, the crack

propagates. In water ice, K_{Ic} = 0.10 to 0.12 MPa m$^{1/2}$ (Liu and Miller, 1979; Andrews, 1985; Bentley et al., 1989). K_I is given by:

$$K_I = \sqrt{\pi\, l}\, [\Delta P - 2\, g\, (\rho_w - \rho_i)\, l/\pi] \quad (3)$$

where the stress intensity decreases with crack length l due to the positive liquid-ice density contrast ($\rho_w - \rho_i$) for water. Cracks propagate upward through the ice shell if either external stresses T overcome both the negative buoyancy and the fracture toughness of the ice: $T > 2g(\rho_w - \rho_i)l/\pi + K_{Ic}/\sqrt{\pi l}$, or if the cryovolcanic fluid is sufficiently less dense than ice ($\rho_w < \rho_i$) that $K_I > K_{Ic}$.

External stress can originate from tides, as on Europa or Enceladus. Overpressures from freezing also generate stress. From our analysis above, $T = dP$ of order 10^6 Pa (for f=1%), is sufficient to drive a crack with length $l > 60$ km. Therefore, pressurization alone can initiate kilometer-sized cracks during freezing of either the entire ocean (Manga and Wang, 2007) or, more easily, water pockets in the ice (Fagents, 2003).

Propagation can occur by positive buoyancy if cracks ascend through a shell denser than pure liquid water. Such a shell can be a clathrate-containing or CO_2 ("dry ice") icy mantle (Lunine and Stevenson, 1985; Crawford and Stevenson, 1988), or even an undifferentiated ice-rock crust (Desch et al., 2009). Positive buoyancy can also occur if the fluid is not pure water, but rather an aqueous solution of volatile species that can decrease fluid density by exsolving during ascent, due to the decreasing confining pressure (Crawford and Stevenson, 1988; Matson et al., 2012). Whether volatile exsolution occurs depends on the volatile composition of cryolavas and on the solubility of these volatiles in water at the temperatures and pressures relevant to KBOs. We focus on these aspects in the following sections.

2.3. Volatile inventory of KBOs

Volatiles are better retained by large bodies (higher gravities) that are distant from the Sun (cold). Dynamical models predict that KBOs formed between 15 and 30 AU away from the Sun (Levison et al., 2008; McKinnon et al., 2008); a simple energy balance calculation reveals that this corresponds to temperatures between 45 and 65 K. Direct comparison between these temperatures and equilibrium condensation temperatures in the solar nebula (Lodders, 2003) to determine which volatiles were accreted is tricky, because the condensation chemistry was likely governed by kinetic processes. In Table 1, the condensation temperatures are provided only for the species that should have condensed under equilibrium. Condensation of the other species in Table 1 was likely kinetically allowed, because they are observed today in comets that should have undergone little endogenic processing, as well as in extrasolar disks. McKinnon et al. (2008) cautioned that any direct extrapolation from present-day comets to volatiles accreted by KBOs overlooks evolutionary effects on cometary volatile-to-water ratios (e.g., Shock and McKinnon, 1993). Interstellar cloud abundances and direct observation of inner extrasolar disk compositions are also biased, because the bulk compositions of extrasolar systems may be widely different from that of the solar system (Young et al., 2014). However, Table 1 reports abundances of CO, H_2O, HCN, and C_2H_6 from a variety of observations of comets (Mumma and Charnley, 2011) that are of same order of magnitude as those observed in extrasolar disks (Maret et al., 2006; Carr and Najita, 2008), although the CO_2 abundances differ significantly. The general consistency between these values provides guidance to estimate primordial volatile abundances in the solar system. Species too volatile to condense at 45 to 65 K, such as primordial Ar, were presumably initially trapped in amorphous ice or as clathrate hydrates. Spectroscopic observations have not revealed any compositional gradient across the inner regions of the Kuiper belt today up to 50 AU (McKinnon et al., 2008), which suggests that significant shuffling of the KBO orbits occurred. Extensive orbital migration is also suggested by dynamical models (Levison et al., 2008).

Early heating on cold bodies may have sublimated the most volatile species, which would have recondensed closer to the surface at colder regions, resulting in a redistribution of volatiles with depth and stratification (Choi et al., 2002; McKinnon, 2002; Prialnik et al., 2008). Past outgassing would have partially depleted the smaller KBOs in volatiles (Choi et al., 2002). However, most volatiles should have been retained in dwarf planets such as Pluto and Charon (McKinnon et al., 2008): H_2 may have been lost (but later produced in water-rock reactions), but N_2 and CH_4 are seen today in the atmospheres of Pluto and Triton (Buratti et al., 1999; Sicardy et al., 2003), and comets of much smaller size than KBOs have retained CO today in large quantities (Mumma and Charnley, 2011). Subsequent softening or melting of ice due to heating by short- and long-lived radionuclides, tidal interactions, differentiation, crystallization of amorphous ice, or exothermic water-rock reactions would have further processed this volatile inventory, potentially concentrating volatile impurities into the aqueous melt (McKinnon et al., 2008). Thus, the icy mantle may be purer water than the liquid layer, whose dissolved volatiles and salts would act as antifreezes to preserve liquid on geological time scales (Desch et al., 2009; Robuchon and Nimmo, 2011). If not dissolved, volatiles could have escaped or could still be outgassing today even on Charon-sized bodies (Choi et al., 2002); this is the process that we investigate in this paper. We review in further detail the current knowledge of primordial abundances and fate of volatile species below.

2.3.1. Carbon species

Carbon in the protoplanetary disk should have been in the form of CO, CO_2, CH_3OH, and CH_4, as well as condensed in refractory C-rich organics. Refractory organics could have taken up to 80% of the total carbon, as suggested by measurements on cometary particles both in-situ at Halley (Fomenkova, 2000) and returned from Wild-2 by the *Stardust* mission (Sandford et al., 2006), as well as by observations of the dark surface of Phoebe, a likely captured KBO (McKinnon, 2002; Castillo-Rogez et al., 2012, and references therein), and by models of the chemical evolution of protoplanetary disks (Kress et al., 2010). This material could make up to 25% of the mass of KBOs (McKinnon et al., 2008).

Of the remaining 20% of the gas-phase C, the values in Table

	Volatile species	Formula	Condensation Temperature (K)[a]	Bulk abundance A_i (mol/mol, % w.r.t. H_2O) Primordial		Endogenic	Canonical model
				Comets[b]	Disk		
O	Water ice	H_2O	121 to 182	100	100		
C	Carbon monoxide	CO		0.4-30	50-100 [c]		20
	Carbon dioxide	CO_2		2-30	0.002-0.26 [c]		10
	Methane	CH_4	78 (hydrate), 41 (pure)	0.4-1.6		Some?	1
	Ethane	C_2H_6		0.01-2	0.008-0.016 [c]		
	Methanol	CH_3OH		0.2-7			3
	Formaldehyde	H_2CO		0.1-1			
	Formic acid	HCOOH		0.06-0.14			
N	Molecular nitrogen	N_2	58 (hydrate)			Some?	1
	Ammonia	NH_3	131 (hydrate)	0.2-1.4	7-14.5 [a,d]		1
	Isocyanic acid	HNCO		0.02-0.1			
	Hydrogen cyanide	HCN		0.01-0.05	0.13-0.26 [c]		
S	Hydrogen sulfide	H_2S		0.12-1.4		Some?	0.5
	Carbonyl sulfide	OCS		0.1-0.4			
	Sulfur dioxide	SO_2		0.002		Some?	0.002
H	Molecular hydrogen	H_2				Most	0.001
Ar	Argon	Ar	48 (clathrate hydrate)	1? [e,f]			0.1

Table 1: Condensation temperatures and typical cometary and disk abundances of volatiles determined by molecular spectroscopy, which explains why abundances of diatomic molecules and noble gases have not been measured. After [a]Lodders (2003), [b]Mumma and Charnley (2011, and references therein), [c]Carr and Najita (2008), [d]Maret et al. (2006), [e]Stern et al. (2000), [f]Bockelee-Morvan et al. (2003). The values from Lodders (2003) represent equilibrium at 10^{-4} bar, but the condensation chemistry of ices was likely governed by kinetic effects.

1 suggest that up to 50-80% was CO (not in equilibrium) at low temperature past Saturn. If much CO and CO_2 were accreted, less oxygen would have been available to form H_2O, yielding denser bodies in regions where rock and ice condensed, but not CO. Conversely, if most of the carbon accreted was refractory, then the initial ice/rock ratio should have been higher than today, implying loss of ices (McKinnon, 2002). CO abundances are observed to be around 20% in comets (Mumma and Charnley, 2011), but only 0.1% on Triton's surface (McKinnon et al., 2008). CO depletion could be due to its consumption in hydrothermal processes (Shock and McKinnon, 1993). CO_2 is absent in KBO spectra; however, it has been observed on the surface of Triton (McKinnon et al., 2008).

Methanol CH_3OH has been suggested to be in pristine material in planetesimals; it should have been accreted at one to several percent with respect to H_2O on Centaurs (Cruikshank et al., 1998) and KBOs (Barucci et al., 2008). Its irradiation products would explain the red colors of both classes of objects (Brown, 2012). However, surface methanol could also be exogenic, resulting from the ultraviolet photolysis of carbon-bearing ices (Castillo-Rogez et al., 2012, and references therein). Methanol is an antifreeze, depressing the melting point of water down to 157 K (Miller and Carpenter, 1964) at 1 bar, or slightly lower temperatures if other antifreezes are present as well (Kargel, 1992).

Finally, methane has been observed on the surfaces of the largest KBOs (Pluto, Quaoar, Eris, Sedna, and Makemake) and Triton (McKinnon et al., 2008). Methane can be produced in water-rock reactions; this process was investigated for Enceladus (Glein et al., 2008). Ethane ice, resulting from the radiative processing of methane, has been observed on Makemake, and perhaps on Orcus and Quaoar (Brown, 2012). Methane could also be the product of hydrothermal alteration of refractory organic matter in heated rocky cores, possibly with a high D/H ratio (Glein et al., 2009).

2.3.2. Nitrogen species

The dominant nitrogen volatiles accreted are ammonia (NH_3) and N_2, and nitrogen was likely also accreted in condensed carbonaceous matter (McKinnon et al., 2008); although which of these three forms dominates is unknown. The previously mentioned analyses of cometary particles revealed C:N ratios of 5 to 50 (Fomenkova, 2000; Sandford et al., 2006). These ratios translate to 0.5 to 5% of the total KBO mass consisting of nitrogen in the form of refractory organics.

NH_3 could have been accreted at one to several percent with respect to H_2O on Centaurs (Cruikshank et al., 1998) and KBOs (Barucci et al., 2008), perhaps as high as 14.5% assuming all N condensed into NH_3 (Lodders, 2003). These estimates are in agreement with observations of extrasolar disks (Maret et al., 2006), although in solar system comets, the ratio NH_3/H_2O is less than 2% (Mumma and Charnley, 2011). NH_3 has been observed on Orcus (de Bergh et al., 2005; Barucci et al., 2008; Carry et al., 2011) and Charon (Brown and Calvin, 2000; Dumas et al., 2001; Cook et al., 2007; Merlin et al., 2010) in amounts relative to water similar to comets. These measurements used the absorption band of ammonia hydrate ices at 2.2 μm. Because this signature is easily masked by the presence of methane, ammonia may be present on other KBOs that display the spectral signature of methane, such as Pluto, Quaoar (Jewitt and Luu, 2004), and Makemake. A similar ammonia-to-water ratio has also been measured in the plume of Enceladus (Waite Jr et al., 2009), and flows of cryolava with this ratio would display morphologies comparable to those observed on

Miranda and Ariel (Thomas et al., 1987; Schenk, 1991); ammonia may have been observed on Miranda (Bauer et al., 2002). Like methanol, ammonia is also an antifreeze and depresses the melting point of water down to 176 K (Leliwa-Kopystynski et al., 2002).

N_2 lacks an electric dipole, therefore its spectral signature is hard to detect and hampers the quantification of its abundance. It is also difficult to distinguish N_2 from CO by mass spectrometry. Bockelee-Morvan et al. (2003) reported upper limits on reliable N_2 measurements of $< 0.2\%$ in comets. N_2 ice is a major surface component on Pluto and Triton, and contributes substantially to their tenuous, seasonal atmosphere. N_2 has also been observed on Sedna and perhaps Eris (McKinnon et al., 2008). N_2 could also be generated by hydrothermal processes on icy bodies (Glein et al., 2008; Mousis et al., 2009). Here, we assume that roughly half of the N accreted by KBOs was in the form of N_2, so that $A_{N2} \approx A_{NH3}$ in Table 1.

The sources and abundances of N in the solar nebula, and the extent to which N compounds may have been accreted by outer solar system bodies, have been reviewed in further detail by Desch et al. (2009).

2.3.3. Sulfur species, hydrogen, and noble gases

Sulfur volatiles of relevance are H_2S and SO_2; both have been observed in comets in small amounts with respect to water (Table 1). Hydrothermal processing of sulfur-bearing minerals also generates these gases. Crawford and Stevenson (1988) pointed out that SO_2 may not concentrate in the aqueous melt, because it is readily trapped in the ice as a clathrate hydrate. SO_2 can also react with water to form sulfurous acid and sulfite species.

It is difficult to envision how dwarf planets could have accreted H_2, unless a small amount was trapped in mixed clathrates or in amorphous ice. However, H_2 is an abundant product of hydrothermal reactions between water and reduced rock. One can estimate an upper limit on the amount of H_2 produced by hydrothermal alteration of the core from the reaction $3\ Fe_2SiO_{4\ (s)} + 9\ Mg_2SiO_{4\ (s)} + 14\ H_2O_{(l)} \rightarrow 2\ Fe_3O_{4\ (s)} + 6\ Mg_3Si_2O_5(OH)_{4\ (s)} + 2\ H_{2\ (g)}$ (i.e., fayalite + forsterite + water → magnetite + serpentine + hydrogen gas). This assumes that the silicate component of KBOs is dry olivine at the time of KBO formation. For Charon (bulk density 1.6 g cm^{-3}), a dry olivine core (density 3.25 g cm^{-3}, accounting for macroporosity) would extend to a radius of about 350 km, with a mass 5.8×10^{20} kg, about half the mass of the icy shell (assuming rock fully differentiates from ice). Since fayalite and forsterite have molar masses of 204 g mol^{-1} and 140 g mol^{-1}, this corresponds to a bulk olivine content of $3.7{\times}10^{21}$ mol inside Charon. If all of it is serpentinized, 6.2×10^{20} mol of H_2 are produced. The molar H_2/H_2O ratio is then about 1%. Thus, considerable quantities of H_2 can in principle be produced. For our canonical simulations, we assume a much smaller amount of 0.001% relative to H_2O, which may correspond to a balance between production and outgassing.

Finally, noble gas observations are sparse for comets. In principle, Ar can be sequestered in amorphous ice to be later accreted during planet formation (Desch and Monga, 2014). Ar was observed in Hale-Bopp at a level of about 1% with respect to water vapor (Stern et al., 2000), but this detection was from a low-resolution spectrum and the spectral line observed may have been due to another species (Bockelee-Morvan et al., 2003). Since Ar has not otherwise been observed on relevant icy bodies, we estimate an Ar abundance from the bulk solar ratio N/Ar ≈ 20 estimated by Lodders (2003).

3. Geochemical model

3.1. Modeling geochemical equilibrium

The purpose of modeling the volatile geochemistry of cryolavas is twofold. First, volatiles can exsolve to make cryolavas positively buoyant, and therefore able to rise spontaneously in ice. Second, geochemical models help constrain the volatile composition of cryolavas. To investigate the propensity of the various volatiles considered in the previous section to exsolve and drive cryovolcanism, we developed a simple chemical model. This model only considers the aqueous and gaseous forms of the volatiles, neglecting volatile speciation into salts or clathrates. It also considers only thermodynamic equilibrium, neglecting kinetic aspects. At chemical equilibrium, the number of moles of a given dissolved volatile per kilogram of water, or molality m, is given by:

$$\log K(T,P) = \log \frac{\gamma_{\text{volatile (aq)}} m_{\text{volatile (aq)}}}{\phi_{\text{volatile (g)}} P_i} \quad (4)$$

where K is the equilibrium (Henry's law) constant for the reaction Volatile (g) → Volatile (aq) at given temperature T and pressure P, γ is the activity coefficient of the solute, and ϕ and P_i are the fugacity coefficient and partial pressure (in bar) of the volatile gas. To evaluate the propensity of volatiles to exsolve as fluid rises, we consider the ideal case of a single volatile dissolved in pure water ($\gamma = 1$). The exsolved gas is assumed to be ideal and composed of the pure volatile ($\phi = 1$ and $P = P_{\text{volatile}}$). The assumption of ideality is reasonable at the low pressures inside KBOs: using the program REFPROP (Lemmon et al., 2010), we calculate a fugacity coefficient $\phi = 1.7$ for N_2 at 240 K and 1000 bar, the upper end of the pressure range encountered in the icy shells of Pluto and Charon.

Each species has a bulk abundance A_i relative to water, determined from Table 1. Provided a crack is open, fluids will spontaneously rise to the level of neutral buoyancy of water ice in liquid water (Crawford and Stevenson, 1988; Matson et al., 2012), such that $z/h = 1 - \rho_i/\rho_w$. Assuming gas absorbs overpressures in the crack, $P_{\text{gas}} = dP$. Let us consider the case where pressurization at the crack tip is just high enough to bring fluid from the neutral buoyancy level (NBL) to the surface: $\Delta P = \rho_i g z$. It follows from equation (2) that $P_{\text{gas}} = dP = \rho_i g h - \rho_w g (h - z)$. We should not assume g to be constant if z or h are not negligible compared to the dwarf planet radius R_p, so $P_{\text{gas}} = \left(\rho_i \int_{Rp-h}^{Rp} g(r)dr\right) - \left(\rho_w \int_{Rp-h}^{Rp-z} g(r)dr\right)$. P_{gas} decreases from the base of the crack and becomes zero at the NBL. Any gas mixture has total pressure P_{gas}, which is the sum of the partial pressures of all mixture components. The

partitioning of each species i between the liquid (m_i) and gas (P_i) is therefore determined by:

$$K_i(T, P) \approx m_i / P_i \tag{5}$$

$$m_i \, \rho_w V_{\rm liq} + P_i V_{\rm gas}/(RT) = A_{i,w} \tag{6}$$

$$\sum_{i=1}^{n_{\rm species}} P_i = P_{\rm gas} \tag{7}$$

In equation (5), we assumed no salinity effect (γ_i = 1 and ϕ_i = 1). If all volatiles are transferred into the liquid as ice melts and refreezes, $A_{i,w} = A_i(1 + M_{\rm ice}/M_{\rm liq})(\rho_w V_{\rm liq}/M_{\rm H2O})$ moles, where $M_{\rm ice}/M_{\rm liq}$ is the ratio of the bulk masses of ice and liquid and $M_{\rm H2O}$ is the molecular mass of water. If not, we just have $A_{i,w} = A_i(\rho_w V_{\rm liq}/M_{\rm H2O})$ moles of volatile i. We use $M_{\rm H2O}$ as the mean molecular mass of the liquid assuming it is mostly water; this no longer holds if the liquid approaches eutectic with an antifreeze. Knowing A_i, T, and $P_{\rm gas}$, and fixing the volumic vapor fraction $x_{\rm vap} = V_{\rm liq}/V_{\rm gas}$, we can solve for all m_i and P_i.

In our models, we fixed $V_{\rm liq}$ as the total volume of liquid water inside the planet, not taking into account other possible liquid species such as ammonia. We conservatively assumed $A_{i,w} = A_i$. The volumic vapor fraction $x_{\rm vap}$ was solved for using equation (7), and the molalities m_i and partial pressures P_i were then calculated using equations (5) and (6). For a detailed description of how the analytical solution to this set of equations was calculated, see Appendix A. Our C routine, "Cryolava", can be freely accessed at https://github.com/MarcNeveu/IcyDwarf.

3.2. Modeling at low temperature and high pressure

An idea of the pressure ranges involved can be obtained from the radial pressure profile for a spherical, homogeneous KBO of density ρ and radius R, given by McKinnon et al. (2008):

$$P(r) \approx 2000 \text{ bar} \left(\frac{\rho}{2\text{g cm}^{-3}}\right)^2 \left(\frac{R}{600\text{km}}\right)^2 \left(1 - \frac{r^2}{R^2}\right) \tag{8}$$

Here, we use units of bar (1 bar = 0.1 MPa), in which geochemical data are referenced. Differentiated bodies will experience slightly higher pressures.

T and P range between about 50 K, 0 bar at the surface and 273 K, $\gtrsim$1 kbar at the base of the ice shell (Desch et al., 2009; Robuchon and Nimmo, 2011). Geochemical codes provide $K(T, P)$ from thermodynamic datasets referenced at 298.15 K and 1 bar, using an equation of state for solutes. The Pitzer (Pitzer, 1973) and HKF (Helgeson et al., 1981, and references therein) equations are commonly used. The former equation has been used down to 173 K in the FREZCHEM code (Marion et al., 2012), but is derived from polynomial fits to experimental data. Thus, it has little predictive power and is restricted to species for which data are available at given T and P. The semi-empirical HKF equation models interactions between solute molecules in water, and does have predictive capabilities.

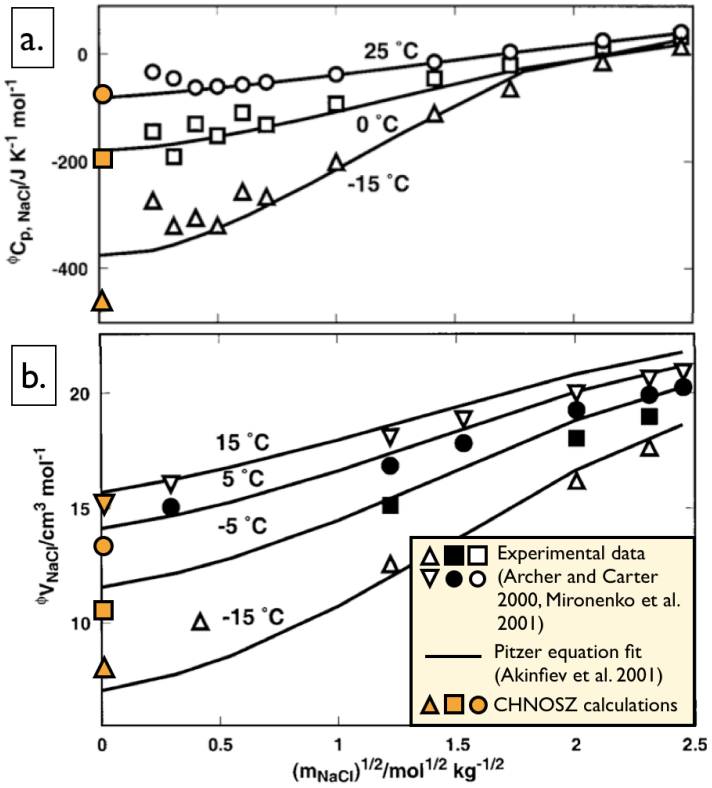

Figure 1: Apparent molar heat capacity (*a.*) and volume (*b.*) of NaCl at subzero temperatures as a function of the square root of the NaCl molality. CHNOSZ predictions at infinite dilution are as accurate as the Pitzer fits (Akinfiev et al., 2001) to experimental data (Archer and Carter, 2000; Mironenko et al., 2001) at low temperature. Modified from Akinfiev et al. (2001).

However, it was developed using data above 273 K. We used the software package CHNOSZ (Dick, 2008) to test the accuracy of the HKF equation down to 253.15 K (the minimum temperature achievable with CHNOSZ) to predict solute properties in supercooled water, and found close agreement with experimental data (Figure 1). Temperatures down to 235 K could be reached using the most up to date equation of state for water, IAPWS-95 (Wagner and Pruss, 2002), in CHNOSZ calculations. Using the IAPWS-95 formulation along with the HKF equation of state makes the model less consistent, because the HKF solute parameters were determined with a previous thermodynamic formulation for water (Haar et al., 1984). However, the CHNOSZ calculations in the temperature range (T>254 K) where both the Haar et al. and IAPWS-95 formulations could be used showed no significant difference in solute properties (Figure 2); therefore we confidently extrapolated our calculations down to 235 K. In the CHNOSZ calculations, we used thermodynamic data from Kelley (1960) and Wagman et al. (1982) for gaseous CH_4, CO_2, Ar, SO_2, N_2, H_2S, H_2, and NH_3; Shock et al. (1989) for aqueous SO_2, N_2, H_2S, H_2, and NH_3; Plyasunov and Shock (2001) for aqueous Ar, CH_4, and CO_2; and Shock (1993) and Shock and McKinnon (1993) for CO.

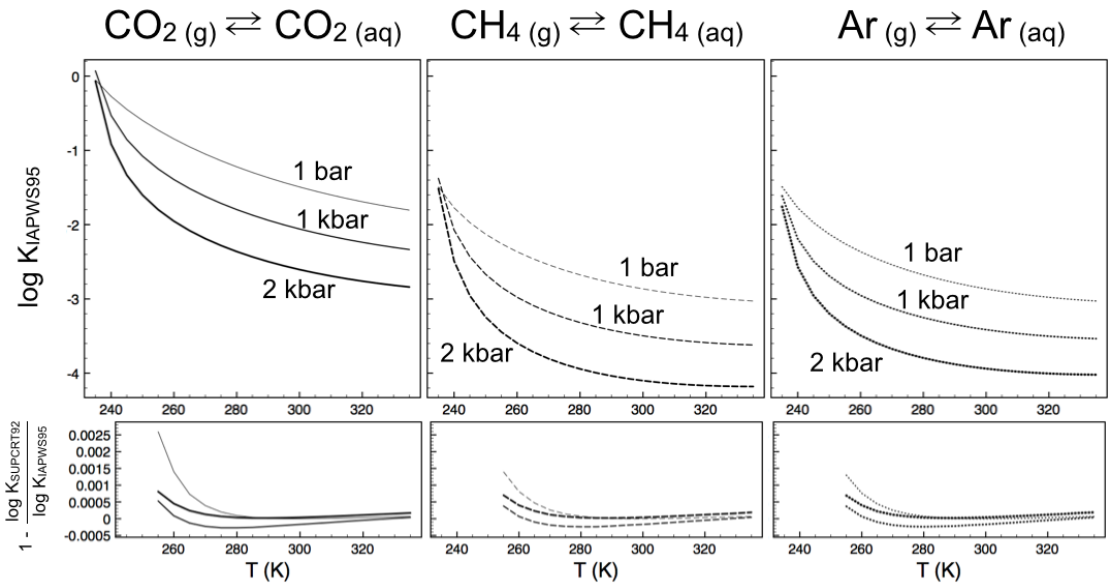

Figure 2: *Top panels:* Logarithm of the equilibrium (Henry's law) constant for the solution of CO_2 (g), CH_4 (g), and Ar (g) as a function of temperature (range 235 K to 335 K) at 1, 1000, and 2000 bar. These predictive curves match experimental data where they exist (above 273 K; Shock et al., 1989). The log K for the other seven species investigated follow similar trends. Note that K, the intrinsic solubility, decreases both with increasing temperature *and* pressure. This linear variation of the logarithm of Henry's law's "constant" with pressure is made explicit in the Krichevsky-Kasarnovsky equation (Krichevsky and Kasarnovsky, 1935). Decreasing pressure causes exsolution mainly because the denominator term in equation (4) decreases, even though log $K(T, P)$ increases. *Bottom panels:* Relative difference in log K estimated using the formulations of water adopted for SUPCRT92 (Haar et al., 1984) and from IAPWS-95 (Wagner and Pruss, 2002). The relative difference is negligible compared to the value of log K, although it increases towards lower temperatures. If log K_{SUPCRT92} versus T curves were plotted on the top panels, they would be indistinguishable from the log K_{IAPWS95} versus T curves.

3.3. Condition for crack propagation

Assuming cracks of length l were initiated by freezing pressurization, exsolution allows further propagation if $K_I > K_{Ic}$. In equation (3), ρ_w is replaced with $\rho_{\mathrm{fluid}} = \rho_w/(1 + x_{\mathrm{vap}})$; the fluid is therefore positively buoyant in ice for $x_{\mathrm{vap}} > 0.07$. Cryovolcanism is considered to occur if (a) exsolution occurs in cracks of length reasonably permitted by freezing pressurization, and (b) cracks propagate all the way to the surface. Therefore, exsolution serves two purposes in this model: it makes cryolavas buoyant in ice (as suggested by Crawford and Stevenson (1988) and Matson et al. (2012)), but also creates a buoyancy force able to disrupt ice and propagate cracks.

4. Results

4.1. Application to Charon

The analytical solution of equations (5-7) enables both the determination of x_{vap} as a function of total gas pressure P_{gas}, which provides the crack propagation condition, as well as the identification of the species that exsolve. We first ran the geophysical code of Desch et al. (2009) for three cases: (a) a "warm Charon" where rock and ice fully differentiate into a mantle of ice and a core of dry rock (density $\rho_{\mathrm{core}} = 3250$ kg m^{-3}, accounting for about 30% macroporosity), perhaps because of a short-lived radionuclide or amorphous ice crystallization heat peak in the first few Myr of Charon's evolution; (b) a colder case in which Charon only partially differentiates, but where the core still warms up enough to be dehydrated; and (c) a scenario where Charon partially differentiates and its core never dehydrates (density $\rho_{\mathrm{core}} = 2350$ kg m^{-3}, including 30% macroporosity). The putative interior structures of dwarf planets have been discussed in further detail elsewhere (Desch et al., 2009; Castillo-Rogez and McCord, 2010; Robuchon and Nimmo, 2011). Despite an assumed ammonia antifreeze content of 1% with respect to water, liquid is not preserved until the present day in scenarios (a) and (c). Therefore, to allow comparisons between all three cases, we ran the geochemical model after 2.5 Gyr of geophysical evolution, when liquid is still present in all cases in the form of an ocean layer 5 to 10 km thick at a depth dependent on the geophysical structure.

The left panels on Figure 3 show the equilibrium molality m of relevant volatiles as a function of depth (or, equivalently, gas pressure P_{gas}) at 235 K, a temperature typical of a Charon subsurface ocean in the geophysical runs. The most apolar species such as H_2, N_2, and Ar, as well as CH_4 and CO, exsolve most easily. CO_2 and H_2S exsolve only in the crust-less scenario (a), and the miscible species SO_2, CH_3OH, and NH_3 do not exsolve at all. These results are not sensitive to the values for the input abundances of these compounds.

On the right panels of Figure 3, the volumic vapor fraction x_{vap} is plotted as a function of depth. The case of canonical abundances is represented by a thick line; other lines indicate half and double volatile concentrations, to outline uncertainties in volatile accretion and possible concentration by melting and refreezing. A polynomial approximation for x_{vap} as a function of depth d for the cases with a crust (b and c) is $x_{\mathrm{vap}} \approx -4 \times 10^{-7} d^3 + 1 \times 10^{-4} d^2 - 0.02d + 1.3$. For case (a), a power law provides a better fit: $x_{\mathrm{vap}} \approx 2400 d^{-1.85}$. The fluid

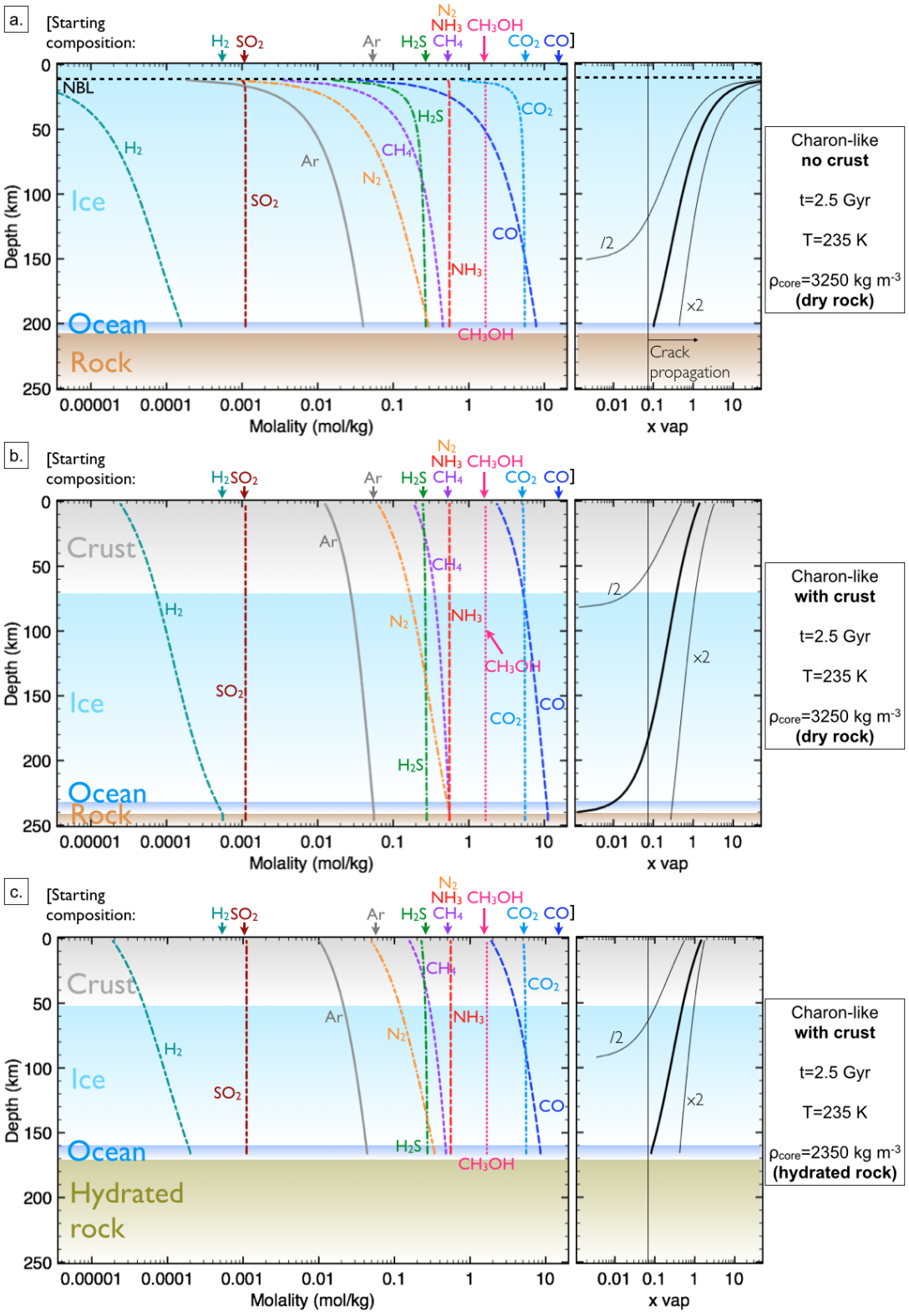

Figure 3: Molality of key volatiles with canonical starting abundances (left panels) and volumic vapor fraction (right panels) as a function of depth for a Charon-like KBO in three scenarios: (a) no crust, dry core; (b) crust, dry core; (c) crust, hydrated core. *Left panels*: The degree to which a species exsolves at a given depth can be estimated by comparing its saturation molality (curve) to its starting concentration, indicated by an arrow at the top of each panel. Low discrepancies indicate that the species is mostly in solution, high discrepancies indicate exsolution. In case (a) where the neutral buoyancy level of water in ice is defined, it is indicated by a dashed line marked "NBL" beyond which calculations were not attempted since $P_{\rm gas} = 0$. *Right panels*: $x_{\rm vap}$ is plotted for the canonical run (thick line), as well as runs with half and twice the abundances (marked "/2" and "x2", respectively). The volumic vapor fraction $x_{\rm vap}$ determines the fluid density $\rho_{\rm fluid} = \rho_w/(1 + x_{\rm vap})$. For $x_{\rm vap} > 0.07$, $\rho_{\rm fluid} < \rho_i$ and $K_I > K_{Ic}$ in cracks of length $l > [\sqrt{\pi}K_{Ic}/(2\Delta\rho g)]^{2/3} \approx 100$ m to 1 km. This limit for crack propagation in ice is indicated as a thin vertical line.

density is then $\rho_{\rm fluid} = \rho_w/(1 + x_{\rm vap})$, neglecting the density of gases. The vertical line on these plots indicates the threshold $x_{\rm vap} > 0.07$ at which fluid becomes positively buoyant in ice. Crack propagation occurs as soon as the fluid is buoyant if cracks are longer than:

$$l > \left(\frac{\sqrt{\pi}\, K_{Ic}}{2\, \Delta\rho\, g}\right)^{2/3} \approx 1\ {\rm km}\left(\frac{10\ {\rm kg\ m^{-3}}}{\Delta\rho}\right)^{2/3} \quad (9)$$

Therefore, assuming canonical abundances, cracks of $l \approx 200$ m, 40 km, and 400 m are needed in cases (a), (b), and (c), respectively. Exsolution is easier without a crust, which acts like a pressure seal to keep the volatiles in solution. It is also easier if the core is hydrated, because the larger volume taken up by the core yields a seafloor closer to the surface. However, the right panels also show that initial abundances, not internal structure, are the main control over crack propagation. In particular, carbon monoxide (CO) plays a major role, because of its combined high abundance and low solubility. Figure 4 shows how sensitive crack propagation is to the initial abundance of CO with respect to water, for each of the three scenarios. With less than 10% CO with respect to water and all other volatile abundances as in Table 1, cracks tens to hundreds of kilometers need to be initiated (presumably by freezing pressurization) for exsolution to drive their propagation further. However, above 15% to 25% CO depending on internal structure, cracks only a few hundred meters high can be propagated by CO exsolution.

4.2. Uncertainty on gas solubilities

The dominant sources of uncertainty for these results are (a) the pressure, temperature, and structure inside Charon, (b) the starting dissolved volatile abundances, (c) the fracture toughness of ice, and (d) the solubility of gases in supercooled water.

We have discussed above the first two sources of uncertainty. Regarding the third one, equation (9) shows that the crack length l scales with the ice fracture toughness as $l \propto K_{Ic}^{2/3}$: varying K_{Ic} over a plausible range of one order of magnitude changes l by less than an order of magnitude. This is less than the dependence of l on internal structure, as shown in Figure 3.

Uncertainties on the solubility of gases obtained by regressions of experimental data above 273 K were estimated by Shock et al. (1989), whose results we used for our extrapolations in the supercooled regime. Shock et al. (1989) estimated a typical uncertainty in standard molar Gibbs energy for neutral species of $\Delta G^{\rm o} \approx 1400$ J/mol at 1000 bar and 500°C. This uncertainty decreases as P and T shift away from the critical point of pure water: at 1000 bar and 25°C, Shock et al. (1989) estimated an uncertainty of only 11 J/mol. When considering a solubility reaction, $\Delta_r G^{\rm o} = G^{\rm o}_{\rm product} - G^{\rm o}_{\rm reactant} = 2.3\ R\ T\ \log(K)$, so the relative uncertainty in K is $\Delta K/K = \Delta[\log K] = 2\ \Delta G^{\rm o}/(2.3\ R\ T)$. Using the worst-case typical uncertainty $\Delta G^{\rm o} \approx 1400$ J/mol and T=235 K, we find $\Delta K \approx 0.6\ K$. Summing the relative uncertainties on K over the ten species considered implies that X in Appendix A, and therefore $x_{\rm vap}$, are determined within one order of magnitude. This is comparable to changing the volatile abundances by a factor of two in Figure 3, and does not significantly impact the results.

5. Discussion

5.1. Comparing the explosiveness of gases

Non-polar species are those that most easily outgas. However, these species are not necessarily abundant and therefore not necessarily the best drivers of explosive cryovolcanism. In order to easily evaluate the capacity of a given species to drive cryovolcanism given its solubility and abundance, we evaluate its contribution to $x_{\rm vap}$, i.e., its mole fraction $X_{i({\rm g})} = P_i/P_{\rm gas}$ in the gas phase. From equation (A.4):

$$X_{i({\rm g})} = \frac{A_{i,w}/M_{\rm liq}}{K_i + x_{\rm vap}/(\rho_w RT)}\frac{1}{P_{\rm gas}} \quad (10)$$

where $A_{i,w}$ is the starting abundance of volatiles in liquid water (in mol), $M_{\rm liq}$ is the mass of liquid, and K_i is the equilibrium constant (which depends on temperature and pressure) for the dissolution of each volatile species i. As expected, X_i decreases with the ratio $K_i = m_i/P_i$. Moreover, X_i is directly proportional to $A_{i,w}$: comparing X_i for two different species allows to solve for an abundance ratio for which these species have the same explosiveness. Because $x_{\rm vap}$ and $K_i(T, P_{\rm gas})$ vary with depth, it is most useful to evaluate both at the threshold depth where positive buoyancy is first reached, even though the composition of the gas does not change significantly with depth. The comparative explosiveness for the ten gases considered in this study is shown in Table 2.

CO is the best driver of cryovolcanism, assuming it is present in KBOs in cometary abundances. Its contribution to the gas exceeds that of CO_2 by nearly two orders of magnitude. N_2, CH_4, and H_2 also exsolve easily, but H_2 plays only a minor role in the runs described above because of its low starting abundance. However, most H_2 is likely to arise from hydrothermal reactions at or below the seafloor, the extent of which is currently unconstrained. Such reactions could result in starting abundances of up to 30%. Charlou et al. (2002) measured abundances of hydrothermal H_2, CH_4, and CO near a seafloor hydrothermal field. The abundances of CH_4 and CO were negligible compared to those inferred from comets. However, Charlou et al. (2002) measured an H_2 abundance of 16 mmol kg^{-1}, or roughly 0.03% by mole with respect to water. Although this is 30 times the abundance we considered, it would bring the explosiveness of H_2 on par with that of H_2S, which only contributes to the exsolved gas in a minor way. CO_2 and N_2 abundances highly depend on the redox state of the ocean (Shock and McKinnon, 1993; Glein et al., 2008). CO_2, even at a high abundance, does not exsolve much. However, assuming that temperatures are high enough to convert all of NH_3 to N_2 (Glein et al., 2008), molecular nitrogen may help drive cryovolcanism (although, in that case, there would be no NH_3 antifreeze and another solute would be required to maintain liquid). The contribution of N_2 to the exsolved gas may also be higher than estimated in Table 2 if we underestimated the unconstrained bulk N abundances of KBOs. Ar potentially has a significant role, but as a noble gas its abundance is difficult to constrain. Sulfur gases only play a minor role. However, Crawford and Stevenson (1988) suggested that SO_2 would stay trapped in clathrates rather than being concentrated in the aqueous melt. These clathrates would

Volatile species	Model abundance	Mole fraction $X_{i(g)}$ at highest depth of positive buoyancy		
	A_i (% w.r.t. H_2O)	(a) No crust, dry core	(b) Crust, dry core	(c) Crust, hydrated core
CO	20	8.8×10^{-1}	7.6×10^{-1}	7.6×10^{-1}
N_2	1	7.0×10^{-2}	7.3×10^{-2}	6.1×10^{-2}
CH_4	1	2.7×10^{-2}	2.1×10^{-2}	2.2×10^{-2}
CO_2	10	1.2×10^{-2}	7.8×10^{-3}	9.2×10^{-3}
Ar	0.1	4.2×10^{-3}	3.5×10^{-3}	3.6×10^{-3}
H_2S	0.5	2.3×10^{-3}	1.3×10^{-3}	1.4×10^{-3}
H_2	0.001	1.0×10^{-4}	1.5×10^{-4}	1.0×10^{-4}
CH_3OH	3	5.0×10^{-5}	2.0×10^{-5}	1.8×10^{-5}
NH_3	1	1.4×10^{-5}	7.0×10^{-6}	7.2×10^{-6}
SO_2	0.002	4.3×10^{-8}	2.8×10^{-8}	3.4×10^{-8}

Table 2: Composition of the gas driving explosive volcanism at the depth where positive buoyancy is reached in the cases (a), (b), and (c) of Figure 3 and for canonical initial abundances.

not only increase the ice density and favor positive buoyancy (see below), but also provide an extra source of gas along the way.

Ultimately, all gas abundances depend on how these volatiles speciate among solid (clathrates, amorphous carbon), solute (dissolved volatiles, carbonates, etc.), and gas phases. For example, clathrates and carbonates potentially represent a large volatile sink. Future work will address the speciation issue, but will first require the extension of predictive speciation models to low temperatures. Regardless of the speciation caveat, this analysis of volatile efficiency in driving cryovolcanism ("explosiveness") is useful to identify the species that matter most.

5.2. *Fate of CO in a subsurface ocean*

CO seems to be a key species that can drive explosive cryovolcanic activity because of its expected high abundance and predicted high solubility in water under conditions relevant to KBOs. Therefore, one aspect worth investigating is the geochemical stability of CO in a subsurface ocean. High concentrations of CO are not stable in liquid water: Shock (1993) found a thermodynamic drive at high temperatures (473 K) and pressures (3500 bar) to either hydrolyze CO to formic acid or formate, or to oxidize CO to CO_2 (presumably via formic acid). Figure 5 shows a similar outcome at 235 K and 1000 bar, at relevant redox conditions. The thermodynamic data on the aqueous species used to make Figure 5 were obtained from Shock et al. (1989) for NH_3 and N_2; Plyasunov and Shock (2001) for methanol, ethanol, and CO_2; Shock and McKinnon (1993) for CO, urea, and HCN; Shock (1995) for formic acid and acetic acid; Dick et al. (2006) for glycine; and Schulte and Shock (1993) for acetaldehyde. The data on minerals were taken from Helgeson et al. (1978). Whether CO accreted by KBOs is destroyed over the geologic history of these bodies depends on the rate at which CO is consumed to form one of these species.

Trump and Miller (1973) determined the kinetics of the formation of formate ($HCOO^-$) from CO according to the reaction:

$$CO_{(aq)} + OH^-_{(aq)} = HCOO^-_{(aq)} \quad (11)$$

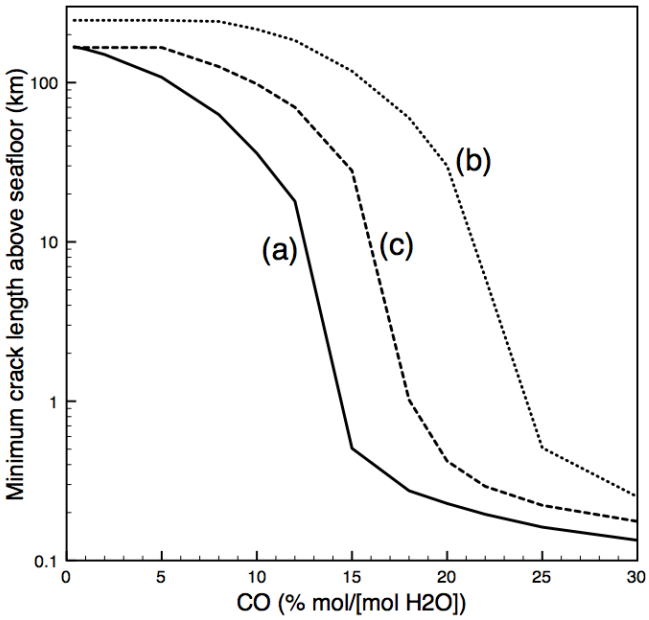

Figure 4: Minimum crack length necessary so that exsolution drives crack propagation, as a function of the initial abundance of carbon monoxide, CO. The scenarios (a), (b), and (c) are the same as in Figure 3.

from 20°C to 60°C. They found the rate data to fit the following equation:

$$\frac{d[\mathrm{CO}]}{dt} = -k_{\mathrm{hyd}}[\mathrm{OH}^-][\mathrm{CO}] \quad (12)$$

with $\log(k_{\mathrm{hyd}}) = 15.83\text{-}4886/T(\mathrm{K})$ M^{-1} h^{-1}, where k_{hyd} represents the second-order rate constant for the alkaline hydrolysis of CO. It appears that Trump and Miller (1973) determined this experimental rate under the assumption of second-order kinetics; reproducing their experiments by adding in turn each of the reactants in excess and confirming the rates to be proportional to each of the reactants would confirm this. However, it seems plausible, mechanistically, that OH^- base would catalyze the reaction by reacting with the electrophilic carbon atom of CO.

Given this rate of CO consumption, the time needed for the concentration of CO to decrease to 10% of its initial value is

given by:

$$t_{10\%} = \frac{\ln(10)}{k_{\rm hyd}[{\rm OH}^-]} \approx \frac{2.3 a_{\rm H+}}{k_{\rm hyd} K_{\rm w}} \quad (13)$$

where $a_{\rm H+}$ corresponds to the activity of H^+, which is equivalent to pH = – log ($a_{\rm H+}$), and $K_{\rm w}$ designates the ionization constant of water (for the reaction $H_2O = H^+ + OH^-$). $K_{\rm w}$ in supercooled water at 1 kbar can be estimated by extrapolating data from SUPCRT92 (Johnson et al., 1992):

$$\log(K_{\rm w}) = 44.27 - 4921/T({\rm K}) - 7.266 \ln(T) \quad (14)$$

The thermodynamic data used to make this extrapolation are from Haar et al. (1984) for H_2O and Shock and Helgeson (1988) for the ions. The neutral pH is $pH_{\rm Neu} = -\log(K_{\rm w}^{0.5})$, and the activity of H^+ at pH relative to neutrality ($pH = pH_{\rm Neu} + x$) can be expressed as $a_{\rm H+} = K_{\rm w}^{0.5} \times 10^{-x}$. Therefore, the characteristic timescale for conversion of CO to formate can be written as:

$$t_{10\%} \approx \frac{2.3 \times 10^{-x}}{k_{\rm hyd} K_{\rm w}^{0.5}} \quad (15)$$

Figure 6 shows the analytical solution of equation (15), $t_{10\%}$, as a function of pH relative to neutral (x). These results should be viewed as having order-of-magnitude quality because of the extrapolation to low temperatures. CO is hydrolyzed faster at higher temperatures and higher pH. If even slightly warm (323 K) hydrothermal systems arose on Pluto or Charon, CO would have been destroyed extremely quickly. Lower pH would allow CO to survive longer. Zolotov (2012) modeled chemical equilibrium between cometary volatiles and CI chondrite solids down to 0°C, and found that the predicted equilibrium pH is about two units above neutrality. The relatively high pH in these systems is dictated by reactions between ultramafic silicate minerals and the aqueous solution. Therefore, supercooled oceans inside KBOs may also have a pH greater than neutrality. However, production of formic acid would decrease the pH. Figure 6 shows that CO should be destroyed rapidly (in terms of geologic time) in such mildly alkaline solutions. Very low temperatures (below 200 K) are required to prevent significant hydrolysis of CO over the age of the solar system. However, exceptionally cold NH_3-H_2O oceans may not preserve CO, as they could be highly alkaline (Marion et al., 2012).

CO is present in the surface reflectance spectra of Pluto-sized KBOs, but not in those of Charon-sized bodies (Brown, 2012, and references therein). Schaller and Brown (2007) argued that this was because a minimum dwarf planet radius of 500 to 700 km was necessary to prevent Jeans escape of CO at KBO surface equivalent temperatures of 30 to 40 K. Surface CO could either never have been in contact with liquid water (and therefore not been hydrolyzed to formate), or could have originated from formate that dissociated into CO and H_2O at the very cold surface temperatures or under irradiation. Therefore, there may be appreciable amounts of CO in the ocean from recent melting of CO-bearing ice. In this case, however, the concentration of CO in the ocean would presumably be much lower than the primordial abundance, so the potential for CO to drive cryovolcanism from an ocean may be diminished.

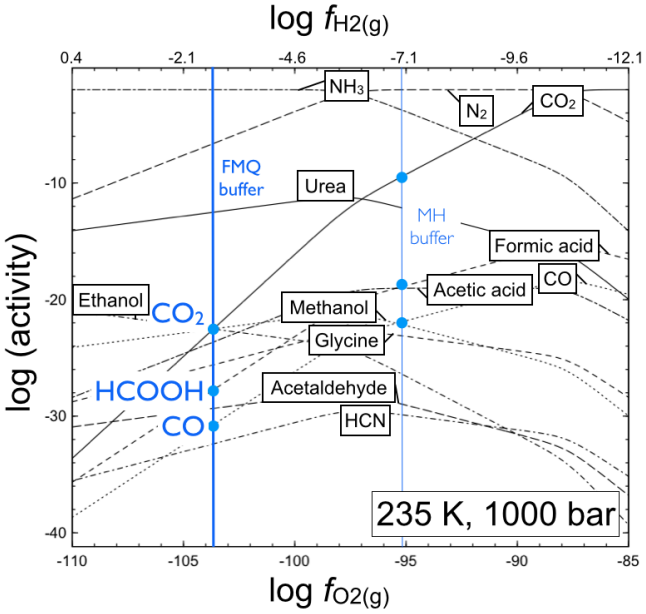

Figure 5: Logarithm of the activities of cometary volatiles, likely to have been accreted by KBOs, as a function of redox conditions in a subsurface ocean at 235 K and 1000 bar. Possible redox conditions are shown by two buffers: the equilibrium between fayalite, magnetite, and quartz ("FMQ"), and that between magnetite and hematite ("MH"). The equilibria between CO and CO_2 and between CO and HCOOH are strongly shifted to the latter species in both cases. Methane is not included in these calculations based on the argument of metastable equilibrium given by Shock and McKinnon (1993).

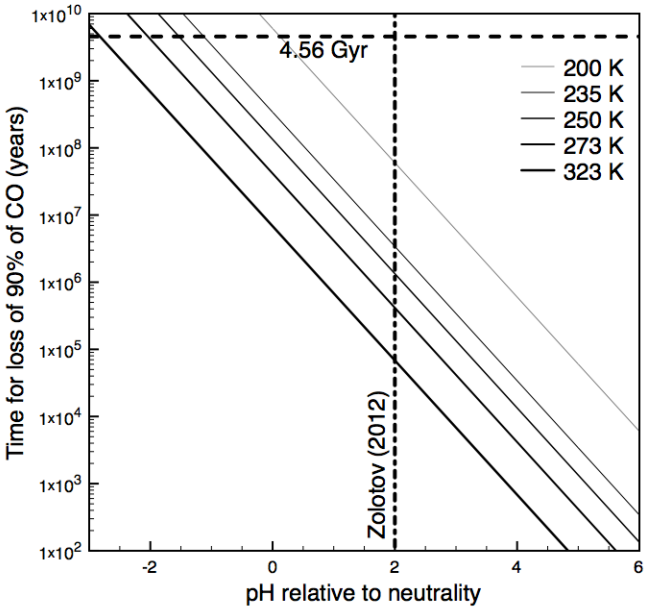

Figure 6: Time after which 90% of aqueous CO is consumed to make formate, as a function of pH relative to neutrality, for temperatures between 200 K and 323 K. Overlain are the age of the solar system (4.56 Gyr) and a plausible pH of KBO subsurface oceans, two units above neutrality, suggested by Zolotov (2012).

5.3. Effect of internal structure

Comparing results between scenarios (a) and (b) yields insights into the influence of a crust on gas-driven crack propagation. Undifferentiated crusts are a surprising outcome of thermal evolution models of KBOs (Desch et al., 2009), because these crusts are denser than the underlying ice mantle. Detailed modeling of the rheology of silicate-ice mixtures has shown that KBOs with a size up to that of Charon remain too cold near the surface for a crust dozens of kilometers thick to founder by Rayleigh-Taylor instabilities over timescales comparable to the age of the solar system (Rubin et al., in review).

In principle, undifferentiated crusts dozens of kilometers thick should *favor* the ascent of fluid-filled cracks, because of the favorable density contrast even when the fluid is pure liquid water. Percolation of methanol- and ammonia-rich cryolavas upward through undifferentiated ice-rock mixtures has indeed been invoked as a mechanism to extrude material that, once irradiated, resembles the red surfaces of many 100 km-class Centaurs and KBOs (McKinnon et al., 2008). However, Charon-sized bodies are still large enough that they experienced partial differentiation into a rocky core and an icy mantle, through which fluid-filled cracks must propagate before reaching the base of the crust. Therefore, fluid pressurization by volatile exsolution or partial freezing remains necessary in the ice mantle.

An outcome of the present study is that undifferentiated crusts *inhibit* exsolution by raising the confining pressure in the icy mantle and the ocean. Higher confining pressures require either longer fluid-filled cracks or higher volatile (CO) abundances for exsolution-driven ascent to occur. Another inhibiting feature of crusts is that their fracture toughness K_{Ic} should be higher than that of ice, given that a crust is an undifferentiated mixture of icy and rocky grains (F. Nimmo, personal communication). How much higher K_{Ic} becomes is difficult to predict, but it could not be higher than its value for hydrated, loosely consolidated rock, about 0.5 MPa $m^{1/2}$ (Chen et al., 2000; Backers, 2005; Tromans and Meech, 2002; Wang et al., 2007), which is higher by a factor of about 5 than the value for pure ice. Finally, near-surface porosity could decrease the crustal density enough to impede ascent through the last kilometers of crust. However, at these shallow depths, gas-dominated fluid should still be buoyant.

Comparing results between scenarios (b) and (c) allows us to investigate the influence of hydration in the core on cryovolcanism. A hydrated core (density similar to that of serpentine rock with a few percent porosity) takes up a larger volume than a dry core (density similar to that of olivine rock with a few percent porosity). A larger, hydrated core results in the ocean being closer to the surface, at lower pressures than in scenario (b). Thus, exsolution is favored in case (c) compared to case (b), although it is not as easy as in case (a) despite the fact that the seafloor is shallower.

5.4. Freezing during ascent

Another issue of fluid ascent is that it needs to be faster than the timescale of its freezing on the channel walls (Desch et al., 2009). This timescale is increased if the liquid contains antifreezes. Stevenson (1982) estimated upward propagation velocities of 1 to 10 cm s^{-1} and 10% of fluid freezing on icy Saturnian satellites of sizes and densities comparable to those of dwarf planets and for crack diameters D of order 10^2 to 10^3 m. From his estimations, we infer a propagation timescale through a 100 km thick ice shell of 10^6 to 10^7 s and a freezing timescale of 10^7 to 10^8 s. However, antifreezes also increase the viscosity of the liquid, which slows it down near the walls. The maximum propagation velocity of a viscous fluid through a pipe is given by:

$$v_{\max} = \frac{D^2}{4\eta}\frac{\partial P}{\partial z} \tag{16}$$

where D is the pipe (crack) diameter, η the fluid viscosity, and $\partial P/\partial z = (\rho_w - \rho_i)\, g$ the hydrostatic pressure gradient. For cracks originating at the base of an ice shell of thickness d overlying a liquid layer, the ascent time scale $\tau_{\text{asc.}} = d/v_{\max}$ is therefore:

$$\tau_{\text{asc.}} = \frac{4\, d\, \eta}{\Delta\rho\, g\, D^2} \tag{17}$$

Kargel (1991, 1992) and Kargel et al. (1991, 2000) studied the composition, rheology, and ascent of cryolavas composed of H_2O, NH_3, CH_3OH, and N_2 that may be liquid down to 155 K. Kargel et al. (1991) determined experimentally that the viscosity of H_2O-NH_3 mixtures is between 10 and 100 Pa s at T=175 to 235 K and X_{NH3} of a few percent up to eutectic composition (32.1%). Adding methanol increases the viscosity up to 10^4 Pa s near the peritectic. These viscosities are much higher than those of water or ammonia alone, mostly because of hydrogen bonding and partial crystallization in the mixtures. For a water-ammonia liquid of viscosity 100 Pa s, $g = 0.3$ m s^{-2}, $d =$ 100km, and a cylindrical channel width D of 1 m, we calculate an ascent time scale of 2.7×10^5 (500 kg $m^{-3}/\Delta\rho$) s.

When ascent is driven by pressurization of freezing water, the pressure gradient can be approximated by $\partial P/\partial z \approx (\beta_w h)^{-1}(\Delta V/V)$, where β_w is the compressibility of pure water, h is the depth of the pocket in the ice shell, and $\Delta V/V$ is the relative shrinkage in volume of the water pocket. With $\beta_w \approx 5 \times 10^{-10}$ Pa^{-1}, $h = 10$ km, and $\Delta V/V = 0.1$, $\partial P/\partial z \approx$ 200 Pa m^{-1}; this is comparable to the buoyancy arising from gas exsolution: $\Delta\rho\, g \approx 150$ Pa m^{-1}.

The timescale of freezing a 1 m column of pure water can be estimated as follows. The specific heat to be conducted away is $H = C_p(T)\, \Delta T + L_{\text{freeze}}$, where $C_p(T)$ is the heat capacity and L_{freeze} is the latent heat of freezing. The timescale of freezing τ_{freeze} is then given by:

$$\tau_{\text{freeze}} \approx \rho_{\text{liq}} \times 1 \times \pi D^2\, H \left(\frac{\partial H}{\partial t}\right)^{-1} = \rho_{\text{liq}} \times 1 \times \pi D^2 \frac{H}{k_{\text{ice}}} \left(\frac{\partial^2 T}{\partial r^2}\right)^{-1} \tag{18}$$

Here, r indicates the horizontal distance away from the center of the crack in cylindrical coordinates. We (crudely) approximate the second derivative term as $\partial^2 T/\partial r^2 \approx [(\Delta T/\Delta r)_{\text{crack-wall}} - (\Delta T/\Delta r)_{\text{wall-ice}}]/\Delta r$. We assume a temperature of 235 K at the center of the column and 100 K at the

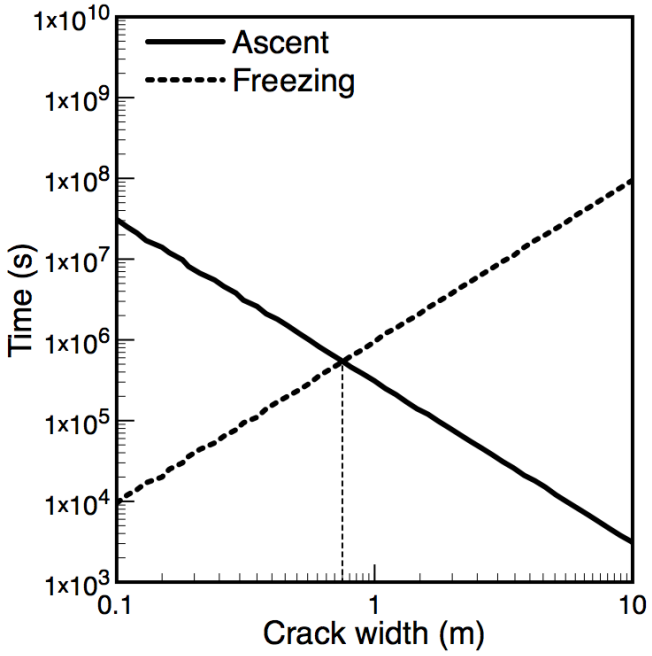

Figure 7: Comparison of timescales for ascent and freezing. The thin dashed line indicates the minimum crack width (diameter) above which propagation through an ice shell is possible before liquid freezes.

walls, as well as 1 m into the ice: $\Delta r = D = 1$ m, $\Delta_{\text{crack-wall}}T = 135$ K, and $\Delta_{\text{wall-ice}}T = 0$ K. Taking $k_{\text{ice}} = 5 * (100K/T) \approx 5$ W K^{-1} m^{-1} (crystalline ice), $C_p \approx 5000$ J K^{-1} kg^{-1} [increases from 4188 to 7000 J/K/kg between 273 K and 230 K, diverges at 228 K for pure water; Archer and Carter (2000)], $L_{\text{freeze}} = 334$ kJ kg^{-1}, and $\Delta T = 235 - 176$ K in the $C_p\Delta T$ term, we estimate $\tau_{\text{freeze}} \approx 1.5\ (\rho_{\text{liq}}/500\text{ kg m}^{-3}) \times 10^6$ s. For pure ammonia, C_p is 4700 J K^{-1} kg^{-1} (Desch et al., 2009), and L_{freeze} for eutectic H_2O-NH_3 is 131.9 kJ kg^{-1}, which yields $\tau_{\text{freeze}} \approx 0.95\ (\rho_{\text{liq}}/500$ kg m$^{-3}) \times 10^6$ s. In addition to freezing because of temperature decrease, there is also the possibility of decompression freezing for pure water ice Ih, which has a negative slope in the P-T phase diagram.

Thus, ascent times are of order 10^5 for both non viscous water (Crawford and Stevenson, 1988) and viscous water-ammonia liquids. This is shorter than the minimum 10^6 s time scale needed for water-ammonia to cool down to 176 K and the latent heat of freezing to be conducted away in crystalline ice. Given the uncertainties in crack geometry, temperatures, material properties, and that we did not consider freezing of the gas component of the fluid, these rough estimates do little more than provide some intuition about the relevant time scales when comparing competing effects on ascent. Figure 7 compares these timescales for various crack widths D. Despite the roughness and uncertainties of the above analysis, the large range of ascent and freezing timescales involved entail a specific threshold crack width, of order 1 m, for successful ascent. It is worth noting that the width of a fracture on Enceladus has recently been estimated at 9 m (Goguen et al., 2013).

Note that ascent happens far too quickly for cracks to heal by solid-state creep of ice. Assuming a crack with $l = 1$m has opened, it would close on a timescale τ_{heal} given by:

$$\tau_{\text{heal}} = \frac{1}{\dot{\epsilon}} = \frac{2\eta}{\sigma} \approx \frac{2\eta\sqrt{\pi l}}{K_{Ic}} = 6\text{ Myr}\left(\frac{\eta}{5\times10^{18}\text{Pa s}}\right) \quad (19)$$

where η is the viscosity of ice, taken from Goldsby and Kohlstedt (2001); $\dot{\epsilon}$ is the strain rate, and σ is the stress. The indicative value of 5×10^{18} Pa s for the ice viscosity is valid for a Pluto- or Charon-sized body at $T \approx 176$ K. This temperature is the eutectic point of a water-ammonia mixture and a likely temperature at the base of the ice shell if volatile antifreezes play any role in maintaining liquid. Near subsurface liquid at 176 K, cracks can remain open for several Myr. At 273 K, the viscosity falls to about 10^{12} Pa s and relaxation occurs in only about one year. Closer to the surface where temperatures are lower and viscosities higher, cracks could remain open over much longer time scales.

5.5. Other model considerations

Several other loosely constrained considerations influence the likelihood of explosive cryovolcanism. First, gas solubility increases with decreasing temperature; this should hamper exsolution during ascent to some extent. Here, we considered the ascent of fluid to be quick enough ($\tau_{\text{asc.}} \approx 0.1\ \tau_{\text{freeze}}$) that the fluid does not have time to cool significantly. In principle, including the temperature effect on solubility should be straightforward, because this effect translates into higher values of $K_i(T, P_{\text{gas}})$ as T decreases. In practice, a predictive geochemical model has yet to be devised for temperatures below that used here, 235 K.

In addition to equilibrium chemical speciation, one should also consider kinetic effects on exsolution. At frigid ocean temperatures, it is possible that speciation and exsolution are inhibited kinetically. To address this uncertainty, experiments in the relevant temperature and pressure regime are necessary, as in the case of explosive silicate volcanism (Mangan and Sisson, 2000). Further insight could be gained from models of nucleation and bubble growth (Yund and McCallister, 1970; Rosner and Epstein, 1972; Sparks, 1978; Proussevitch and Sahagian, 1998) applied to the case of volatiles in aqueous solutions. Exsolution kinetics slower than freezing time scales would keep volatiles trapped into the ice.

Scarce experimental data on supercooled solutes make equilibrium calculations below 235 K speculative. The HKF model for determining solute properties becomes singular at 228 K, where supercooled water seems to have a liquid-liquid critical point near 1 bar (Speedy and Angell, 1976). However, this diverging behavior was not observed at higher pressures, where measurements of supercooled water properties have recently been made possible down to 200 K and up to 4000 bar thanks to improvements in experimental setups (Mishima, 2010). This progress in the experimental determination of supercooled water properties is in turn driving efforts to extend the equation of state of supercooled water in this temperature and pressure regime (Holten et al., 2012). A next logical step would be to update the HKF equation for aqueous solutes, which depends

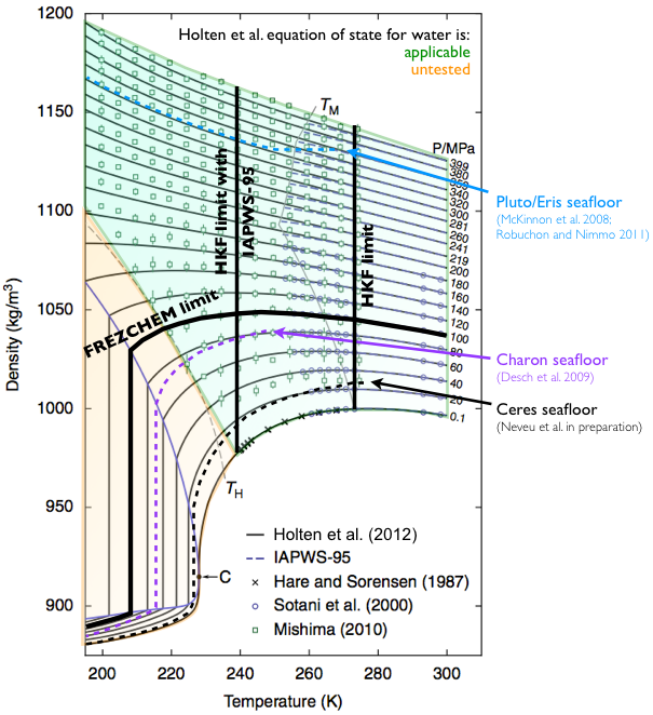

Figure 8: Applicability of current geochemical codes in the pressure-temperature-density (P–T–ρ) space of relevance to icy dwarf planets, delimited by the ammonia-water eutectic point at 176 K (Leliwa-Kopystynski et al., 2002) and the seafloor pressure for Pluto-sized bodies (4000 bar or 400 MPa). The thin solid black curves are predictions of an improved equation of state for water (Holten et al., 2012) that accurately describes measurements from Mishima (2010) and others. Overlain are the geotherms of Ceres- to Pluto-sized dwarf planets (dashed curves), starting at the seafloor and moving through lower T and P to the surface. Seafloor conditions are at the limit of current geochemical codes, such as FREZCHEM and HKF-based CHNOSZ, but theoretical improvements are needed in order to push models to lower T and higher P. Figure modified from Holten et al. (2012).

on the equation of state for water, to account for these improvements, and fit solute properties to existing experimental solute data. This would enable HKF-based codes such as CHNOSZ to compute predictions for properties of species that have not been experimentally characterized (Figure 8).

Extension to a higher pressure regime would enable studies of larger icy bodies. McKinnon et al. (2008) noted that there are no dynamical arguments against larger KBOs the size of Mars or the Earth further away from the Sun. Their study is hampered because current geochemical models are capped at pressures of several thousand bars, the pressures reached near the center of Pluto-sized bodies. A recent model (Facq et al., 2014) has extended the predictive HKF framework to explore the solubility and speciation of carbonate species up to 80 kbar; however, this model cannot currently be used at subzero temperatures. Exoplanets, likely icy, of super-Earth size have also been discovered (Beaulieu et al., 2006). The extension of aqueous geochemical models to higher pressures than present would provide a valuable tool to model the interior of such bodies. When modeling gas exsolution at higher pressures, one should keep in mind that the assumption of ideality is no longer valid: using the program REFROP, we calculate fugacity coefficients for N_2 at 240 K of 1.7 at 1 kbar, 6.1 at 2 kbar, 22 at 3 kbar, 81 at 4 kbar, and 284 at 5 kbar. Large fugacity coefficients make real gases more soluble (less likely to outgas) than ideal gases.

Finally, we have neglected any speciation of dissolved gases (e.g., CO_2 to bicarbonate and carbonate), clathration, and volatile condensation (e.g., CO_2 has a critical point at 304 K). These three phenomena are volatile sinks, decreasing the amount of gas available to form a buoyant fluid. For example, calculations using REFROP show that the fugacity of CO_2 $f_{CO2} = (\phi_{CO2} P_{CO2})$ is only 70 bars at 1 kbar and 240 K. The fugacity of CO_2 cannot keep increasing up to the total pressure; instead, it condenses during ascent once the system pressure approaches this fugacity, preventing further increases in the fugacity. On the other hand, pickup of condensed volatile pockets or clathrates by cryovolcanic fluids during ascent could increase their gas content (Battaglia et al., in preparation).

5.6. *Predictions for Pluto and Charon*

The time scale of cryovolcanic activity on Pluto and Charon-sized KBOs depends on the time at which last freezing occurs, if freezing of water pockets indeed initiates cracks (Fagents, 2003; Manga and Wang, 2007). In the Kuiper belt, dwarf planet oceans are predicted to freeze entirely after a few billion years (Desch et al., 2009; Robuchon and Nimmo, 2011), perhaps about 1 Gyr ago for Charon (Rubin et al., in review; Desch, this issue). Cryovolcanic activity could be sustained over the time needed to freeze a given liquid volume. Assuming a liquid layer several kilometers thick, which corresponds to a eutectic H_2O-NH_3 ocean on Charon if the bulk NH_3 content of the ice was initially 1%, this time could be a few hundred million years (Desch et al., 2009; Rubin et al., in review). Additional activity is expected from freezing of localized water pockets closer to the surface. If such pockets occur, their presumed volume, much smaller than that of a global ocean layer, would sustain cryovolcanism for a correspondingly shorter time: roughly 50 years for a spherical pocket 1 km in radius. If freezing pressurization drives a cryovolcanic outflow, no more than 7% of the freezing volume (i.e., $\rho_w/\rho_i - 1$) may be erupted. With the same assumptions as above, cryovolcanism resulting from global ocean freezing could in principle emplace a global layer up to a kilometer thick on Charon's surface. In practice, one can expect the efficiency of cryovolcanism as a resurfacing process to be orders of magnitude lower.

Plumes arising from explosive cryovolcanism may be observed on Pluto or Charon by the *New Horizons* probe. These plumes may be rich in CO, since this volatile could make up 80% of the exsolved gas and a few percent to tens of percent of the water- and antifreeze-rich material ejected. However, the calculated short lifetime of CO in a subsurface ocean implies that the gas may be generated by near-surface sublimation of CO ice, vaporization of subsurface liquid CO, or eruption of a recent cryovolcanic aqueous melt that is disconnected from the ocean.

Plumes rich in the reduced gases CH_4, H_2, and perhaps N_2 would be evidence for hydrothermal activity inside Pluto or Charon. H_2 does not have a spectral signature in the visible and

near-infrared regions covered by the *Ralph* package, *New Horizons*'s visible and near-infrared spectrometers (Reuter et al., 2008). However, lines resulting from the dissociation of H_2 molecules could be seen in *Alice* ultraviolet spectra (Stern et al., 2008). More generally, each of the ten gases investigated in this study, if abundant enough, can be detected by least one of these instruments.

N_2 plumes could also be evidence that Pluto and Charon accreted rich in N. However, because Pluto's surface and atmosphere are rich in N_2, it will be difficult to assess the origin of such plumes, which could also arise from frost sublimation on the surface as observed on Triton. The co-detection of other gases along with N_2 could be an argument in favor of a deep origin; conversely, plumes of frost composition would likely originate in surface layers. Hydrothermally produced H_2, CH_4, and N_2 may be distinguished from primordial species by their isotopically heavy makeup (Glein et al., 2009; Rousselot et al., 2014).

In addition, evidence for recent explosive cryovolcanism may be gathered from the detailed composition of the surfaces, atmospheres, or exospheres of Pluto and Charon. The fate of cryovolcanic products (condensation or escape) depends on equilibrium and kinetic constraints similar to those during primordial accretion. Species such as CO, CO_2, CH_4, or N_2 could condense back on the surface depending on surface temperature and gravity (Schaller and Brown, 2007), whereas H_2 would certainly escape. The extent to which a given volatile may condense back to the surface could be more precisely estimated if *New Horizons* measurements constrain the rate of processes such as Jeans escape, hydrodynamic escape, and ultraviolet photolysis (Schaller and Brown, 2007). Such measurements include atmospheric thermal profiles (to constrain heating from extreme ultraviolet radiation) and structure (in particular, the exobase altitude from which escape may take place), as well as ejection velocity in potential plumes. *New Horizons* is well equipped to perform such measurements: ultraviolet spectra and atmospheric maps will be acquired by the *Alice* instrument (Stern et al., 2008); atmospheric temperature and structure profiles will be inferred from radio occultations using *REX* (Tyler et al., 2008); and *SWAP* (McComas et al., 2008) and *PEPSSI* (McNutt et al., 2008) will be used to perform solar wind measurements and energetic particle spectrometry to determine *in situ* escape rates (Stern and Spencer, 2003).

Past cryovolcanism may have been the source of methane for Pluto's atmosphere and frosts; this would mean that its past or current ocean had a very reduced composition. On the other hand, mild heating of subsurface clathrate hydrates may suffice to concentrate guest species at the surface. Miscible species such as CH_3OH or NH_3 are not expected to exsolve, but they play a key role in maintaining liquid as antifreezes, and would be entrained by the gas onto the surface during an eruption. Local concentrations of these species would be evidence for extrusion of material from the interior; however, their cryovolcanic origin (i.e., surface deposition as a fluid) would likely be as ambiguous as previous interpretations of similar features on other icy bodies.

6. Conclusions

In this study, we investigated gas exsolution as a mechanism to drive cryovolcanism. We used a novel approach that couples geophysics and geochemistry, and extended geochemical modeling to the seldom-explored realm of liquid water at subzero temperatures. We showed that, provided liquid and crack initiation (e.g. by freezing pressurization), cryovolcanism can occur on dwarf planet-sized KBOs.

CO seems to be an excellent driver for explosive venting, whereas species such as CO_2 and sulfur gases are not. Primordial N accreted as N_2 could also drive cryovolcanism if its abundance, currently unconstrained, is above a few percent with respect to water. CH_4 and H_2 resulting from hydrothermal activity at the putative seafloors of KBOs may also trigger cryovolcanism if they are present in substantial amounts (a few percent with respect to water). The miscible antifreezes CH_3OH and NH_3 remain in solution; this allows persistence of liquid at temperatures well below 200 K.

Therefore, the onset of explosive cryovolcanism hinges mainly on the abundances of CO, N_2, CH_4, and H_2: abundances of a few percent in solution for at least one of these seem necessary to initiate exsolution even in the most favorable settings. This requires at least one of the following scenarios: (a) CO does not get destroyed in an ocean, (b) the quantity of N accreted is at the high end of current estimates, or (c) large amounts of reduced gases are produced by vigorous hydrothermal activity.

Undifferentiated crust that never overturned inhibits exsolution and cryovolcanism by acting as a pressure seal. This finding contradicts previous predictions that crusts provide a favorable medium for fluid-filled crack propagation because of the positive fluid buoyancy. Cryovolcanism is favored if the rocky core is hydrated, because the core then takes up a larger volume and places the seafloor closer to the surface; this reduces the pressure solubilization of volatiles. Other considerations, such as ice relaxation of cracks and fluid freezing during ascent, may hamper cryovolcanism, but rough calculations showed that they do not prevent it if crack propagation happens quickly enough. Therefore, current or recent explosive cryovolcanism is expected on Pluto and Charon if either currently has a subsurface liquid layer, a plausible outcome of thermal evolution models. If this is the case, the icy dwarf planets of the Kuiper belt may well join the list of potentially habitable bodies in the solar system.

7. Acknowledgements

We thank J. M. Dick for modifying the CHNOSZ R geochemistry package to work at subzero temperatures, and D. C. Napolitano and A. D. Edwards for helping with preliminary CHNOSZ calculations. Comments from two reviewers helped significantly improve the "Predictions for Pluto and Charon" section of this manuscript. M. Neveu is grateful to the Keck Institute of Space Studies for hosting him during part of this study. This work was supported by the NASA Astrobiology Institute node at Arizona State University.

8. References

Akinfiev, N. N., Mironenko, M. V., Grant, S. A., 2001. Thermodynamic properties of NaCl solutions at subzero temperatures. Journal of Solution Chemistry 30 (12), 1065–1080.

Andrews, R., 1985. Measurement of the fracture toughness of glacier ice. Journal of Glaciology 31 (108).

Archer, D. G., Carter, R. W., 2000. Thermodynamic properties of the NaCl+H_2O system. 4. Heat capacities of H_2O and NaCl (aq) in cold-stable and supercooled states. The Journal of Physical Chemistry B 104 (35), 8563–8584.

Backers, T., 2005. Fracture toughness determination and micromechanics of rock under mode I and mode II loading. Ph.D. thesis, Universitätsbibliothek.

Barucci, M., Merlin, F., Guilbert, A., De Bergh, C., Alvarez-Candal, A., Hainaut, O., Doressoundiram, A., Dumas, C., Owen, T., Coradini, A., 2008. Surface composition and temperature of the TNO Orcus. Astronomy and Astrophysics 479 (1), L13–L16.

Bauer, J. M., Roush, T. L., Geballe, T. R., Meech, K. J., Owen, T. C., Vacca, W. D., Rayner, J. T., Jim, K. T., 2002. The near infrared spectrum of Miranda: Evidence of crystalline water ice. Icarus 158 (1), 178–190.

Beaulieu, J.-P., Bennett, D., Fouqué, P., Williams, A., Dominik, M., Jørgensen, U., Kubas, D., Cassan, A., Coutures, C., Greenhill, J., et al., 2006. Discovery of a cool planet of 5.5 Earth masses through gravitational microlensing. Nature 439 (7075), 437–440.

Bentley, D., Dempsey, J., Sodhi, D., Wei, Y., 1989. Fracture toughness of columnar freshwater ice from large scale DCB tests. Cold regions science and technology 17 (1), 7–20.

Bockelee-Morvan, D., Crovisier, J., Mumma, M. J., Weaver, H. A., 2003. The Composition of Cometary Volatiles. University of Arizona Press, pp. 391–423.

Brown, M. E., 2012. The compositions of Kuiper belt objects. Annual Review of Earth and Planetary Sciences 40 (1), 467–494.

Brown, M. E., Calvin, W. M., 2000. Evidence for crystalline water and ammonia ices on Pluto's satellite Charon. Science 287 (5450), 107–109.

Brown, R., Kirk, R., Johnson, T., Soderblom, L., 1990. Energy sources for Triton's geyser-like plumes. Science 250 (4979), 431–435.

Buie, M. W., Grundy, W. M., Young, E. F., Young, L. A., Stern, S. A., 2006. Orbits and photometry of Pluto's satellites: Charon, S/2005 P1, and S/2005 P2. The Astronomical Journal 132 (1), 290.

Buratti, B. J., Hicks, M. D., Newburn Jr, R. L., 1999. Does global warming make Triton blush? Nature 397 (6716), 219–219.

Carr, J. S., Najita, J. R., 2008. Organic molecules and water in the planet formation region of young circumstellar disks. Science 319 (5869), 1504–1506.

Carry, B., Hestroffer, D., DeMeo, F. E., Thirouin, A., Berthier, J., Lacerda, P., Sicardy, B., Doressoundiram, A., Dumas, C., Farrelly, D., Müller, T. G., 2011. Integral-field spectroscopy of (90482) Orcus-Vanth. A&A 534, A115.

Castillo-Rogez, J. C., Johnson, T., Thomas, P., Choukroun, M., Matson, D., Lunine, J., 2012. Geophysical evolution of Saturns satellite Phoebe, a large planetesimal in the outer Solar System. Icarus 219 (1), 86–109.

Castillo-Rogez, J. C., McCord, T. B., 2010. Ceres evolution and present state constrained by shape data. Icarus 205 (2), 443 – 459.

Charlou, J., Donval, J., Fouquet, Y., Jean-Baptiste, P., Holm, N., 2002. Geochemistry of high H_2 and CH_4 vent fluids issuing from ultramafic rocks at the Rainbow hydrothermal field (36^o 14" N, MAR). Chemical Geology 191 (4), 345–359.

Chen, C., Lan, G., Tuan, W., 2000. Preparation of mullite by the reaction sintering of kaolinite and alumina. Journal of the European Ceramic Society 20 (14), 2519–2525.

Choi, Y.-J., Cohen, M., Merk, R., Prialnik, D., 2002. Long-term evolution of objects in the Kuiper belt zone: Effects of insolation and radiogenic heating. Icarus 160 (2), 300 – 312.

Clauser, C., Huenges, E., 1995. Thermal conductivity of rocks and minerals. AGU reference shelf 3, 105–126.

Cook, J. C., Desch, S. J., Roush, T. L., Trujillo, C. A., Geballe, T. R., 2007. Near-infrared spectroscopy of Charon: Possible evidence for cryovolcanism on Kuiper belt objects. The Astrophysical Journal 663 (2), 1406.

Crawford, G. D., Stevenson, D. J., 1988. Gas-driven water volcanism and the resurfacing of Europa. Icarus 73 (1), 66 – 79.

Croft, S., Lunine, J., Kargel, J., 1988. Equation of state of ammonia-water liquid: Derivation and planetological applications. Icarus 73 (2), 279 – 293.

Cruikshank, D., Roush, T., Bartholomew, M., Geballe, T., Pendleton, Y., White, S., III, J. B., Davies, J., Owen, T., de Bergh, C., Tholen, D., Bernstein, M., Brown, R., Tryka, K., Ore, C. D., 1998. The composition of centaur 5145 Pholus. Icarus 135 (2), 389–407.

de Bergh, C., A. Delsanti, G. P. Tozzi, E. Dotto, A. Doressoundiram, M. A. Barucci, 2005. The surface of the transneptunian object 90482 Orcus. Astronomy and Astrophysics 437 (3), 1115–1120.

De Sanctis, M. C., Capria, M. T., Coradini, A., 2001. Thermal evolution and differentiation of Edgeworth-Kuiper belt objects. Astronomical Journal 121, 2792–2799.

Delsanti, A., Merlin, F., Guilbert-Lepoutre, A., Bauer, J., Yang, B., Meech, K. J., 2010. Methane, ammonia, and their irradiation products at the surface of an intermediate-size KBO? Astronomy and Astrophysics 520, A40.

Desch, S., Monga, N., 2014. Jupiter's noble gas abundances may require external UV irradiation of the solar nebula. In: Lunar and Planetary Institute Science Conference Abstracts. Vol. 45. p. 1725.

Desch, S. J., this issue. Density of Charon formed from a disk generated by the impact of partially differentiated bodies. Icarus.

Desch, S. J., Cook, J. C., Doggett, T., Porter, S. B., 2009. Thermal evolution of Kuiper belt objects, with implications for cryovolcanism. Icarus 202 (2), 694 – 714.

Dick, J. M., 2008. Calculation of the relative metastabilities of proteins using the CHNOSZ software package. Geochem. Trans 9 (10).

Dick, J. M., LaRowe, D. E., Helgeson, H. C., 2006. Temperature, pressure, and electrochemical constraints on protein speciation: Group additivity calculation of the standard molal thermodynamic properties of ionized unfolded proteins. Biogeosciences 3 (3), 311–336.

Dumas, C., Terrile, R. J., Brown, R. H., Schneider, G., Smith, B. A., 2001. Hubble space telescope NICMOS spectroscopy of Charon's leading and trailing hemispheres. The Astronomical Journal 121 (2), 1163.

Duxbury, N., Brown, R., 1997. The role of an internal heat source for the eruptive plumes on Triton. Icarus 125 (1), 83–93.

Facq, S., Daniel, I., Montagnac, G., Cardon, H., Sverjensky, D. A., 2014. In situ raman study and thermodynamic model of aqueous carbonate speciation in equilibrium with aragonite under subduction zone conditions. Geochimica et Cosmochimica Acta.

Fagents, S. A., 2003. Considerations for effusive cryovolcanism on Europa: The post-Galileo perspective. J. Geophys. Res. 108 (E12), 5139.

Fomenkova, M. N., 2000. On the organic refractory component of cometary dust. In: Composition and Origin of Cometary Materials. Springer, pp. 109–114.

Geissler, P., 2000. Cryovolcanism in the outer solar system. Encyclopedia of Volcanoes, edited by H. Sigurdsson, Academic, San Diego, Calif, 785–800.

Glein, C. R., Desch, S. J., Shock, E. L., 2009. The absence of endogenic methane on Titan and its implications for the origin of atmospheric nitrogen. Icarus 204 (2), 637 – 644.

Glein, C. R., Zolotov, M. Y., Shock, E. L., 2008. The oxidation state of hydrothermal systems on early Enceladus. Icarus 197 (1), 157–163.

Goguen, J. D., Buratti, B. J., Brown, R. H., Clark, R. N., Nicholson, P. D., Hedman, M. M., Howell, R. R., Sotin, C., Cruikshank, D. P., Baines, K. H., Lawrence, K. J., Spencer, J. R., Blackburn, D. G., 2013. The temperature and width of an active fissure on Enceladus measured with *Cassini* VIMS during the 14 April 2012 South Pole flyover. Icarus 226 (1), 1128–1137.

Goldsby, D. L., Kohlstedt, D. L., 2001. Superplastic deformation of ice: Experimental observations. J. Geophys. Res. 106 (B6), 11017–11030.

Haar, L., Gallagher, J. S., Kell, G. S., 1984. NBS-NRC Steam Tables: Thermodynamics And Transport Properties and Computer Programs for Vapor and Liquid States of Water in SI Units. Taylor & Francis Group.

Hansen, C. J., Esposito, L., Stewart, A., Colwell, J., Hendrix, A., Pryor, W., Shemansky, D., West, R., 2006. Enceladus' water vapor plume. Science 311 (5766), 1422–1425.

Hedman, M. M., Gosmeyer, C. M., Nicholson, P. D., Sotin, C., Brown, R. H., Clark, R. N., Baines, K. H., Buratti, B. J., Showalter, M. R., 2013. An observed correlation between plume activity and tidal stresses on Enceladus. Nature, 3 pp.

Helgeson, H. C., Delany, J. M., Nesbitt, H. W., 1978. Summary and critique of the thermodynamic properties of rock-forming minerals. Amer. J. Sci. 278, 1–229.

Helgeson, H. C., Kirkham, D. H., Flowers, G. C., 1981. Theoretical prediction of the thermodynamic behavior of aqueous electrolytes by high pressures and temperatures; IV, Calculation of activity coefficients, osmotic coefficients, and apparent molal and standard and relative partial molal properties to 600 degrees C and 5kb. American Journal of Science 281 (10), 1249–

1516.
Holten, V., Bertrand, C., Anisimov, M., Sengers, J., 2012. Thermodynamics of supercooled water. The Journal of chemical physics 136, 094507.
Ingersoll, A. P., Tryka, K. A., 1990. Triton's plumes: The dust devil hypothesis. Science 250 (4979), 435–437.
Jewitt, D. C., Luu, J., 2004. Crystalline water ice on the Kuiper belt object (50000) Quaoar. Nature 432 (7018), 731–733.
Johnson, J. W., Oelkers, E. H., Helgeson, H. C., 1992. SUPCRT92: A software package for calculating the standard molal thermodynamic properties of minerals, gases, aqueous species, and reactions from 1 to 5000 bar and 0 to 1000°C. Computers & Geosciences 18 (7), 899–947.
Kargel, J., Croft, S., Lunine, J., Lewis, J., 1991. Rheological properties of ammonia-water liquids and crystal-liquid slurries: Planetological applications. Icarus 89 (1), 93–112.
Kargel, J. S., 1991. Brine volcanism and the interior structures of asteroids and icy satellites. Icarus 94 (2), 368–390.
Kargel, J. S., 1992. Ammonia-water volcanism on icy satellites: Phase relations at 1 atmosphere. Icarus 100 (2), 556–574.
Kargel, J. S., Kaye, J. Z., Head, J. W., Marion, G. M., Sassen, R., Crowley, J. K., Ballesteros, O. P., Grant, S. A., Hogenboom, D. L., 2000. Europa's crust and ocean: Origin, composition, and the prospects for life. Icarus 148 (1), 226–265.
Kelley, K. K., 1960. High-temperature heat-content, heat-capacity, and entropy data for the elements and inorganic compounds. US Govt. Print. Off.
Kirk, R., Soderblom, L., Brown, R., Kieffer, S., Kargel, J., 1995. Triton's plumes: discovery, characteristics, and models. In: Neptune and Triton. Vol. 1. pp. 949–989.
Klinger, J., 1980. Influence of a phase transition of ice on the heat and mass balance of comets. Science 209, 271.
Kress, M. E., Tielens, A. G., Frenklach, M., 2010. The soot line: Destruction of presolar polycyclic aromatic hydrocarbons in the terrestrial planet-forming region of disks. Advances in Space Research 46 (1), 44–49.
Krichevsky, I., Kasarnovsky, J., 1935. Thermodynamical calculations of solubilities of nitrogen and hydrogen in water at high pressures. Journal of the American Chemical Society 57 (11), 2168–2171.
Küppers, M., O'Rourke, L., Bockelée-Morvan, D., Zakharov, V., Lee, S., von Allmen, P., Carry, B., Teyssier, D., Marston, A., Müller, T., et al., 2014. Localized sources of water vapour on the dwarf planet (1)[thinsp] ceres. Nature 505 (7484), 525–527.
Le Corre, L., Le Mouélic, S., Sotin, C., Combe, J.-P., Rodriguez, S., Barnes, J., Brown, R., Buratti, B., Jaumann, R., Soderblom, J., et al., 2009. Analysis of a cryolava flow-like feature on Titan. Planetary and Space Science 57 (7), 870–879.
Leliwa-Kopystynski, J., Maruyama, M., Nakajima, T., 2002. The water-ammonia phase diagram up to 300 MPa: Application to icy satellites. Icarus 159 (2), 518 – 528.
Lemmon, E. W., Huber, M. L., McLinden, M. O., 2010. NIST Reference Fluid Thermodynamic and Transport Properties - REFPROP. NIST.
Levison, H. F., Morbidelli, A., VanLaerhoven, C., Gomes, R., Tsiganis, K., 2008. Origin of the structure of the Kuiper belt during a dynamical instability in the orbits of Uranus and Neptune. Icarus 196 (1), 258 – 273.
Liu, H. W., Miller, K. J., 1979. Fracture toughness of fresh-water ice. Journal of Glaciology 22, 135–143.
Lodders, K., 2003. Solar system abundances and condensation temperatures of the elements. The Astrophysical Journal 591 (2), 1220.
Lopes, R., Mitchell, K., Stofan, E., Lunine, J., Lorenz, R., Paganelli, F., Kirk, R., Wood, C., Wall, S., Robshaw, L., et al., 2007. Cryovolcanic features on Titan's surface as revealed by the Cassini Titan Radar Mapper. Icarus 186 (2), 395–412.
Lunine, J., Stevenson, D., 1985. Thermodynamics of clathrate hydrate at low and high pressures with application to the outer solar system. The Astrophysical Journal Supplement Series 58, 493–531.
Manga, M., Wang, C.-Y., 2007. Pressurized oceans and the eruption of liquid water on Europa and Enceladus. Geophysical research letters 34 (7), L07202.
Mangan, M., Sisson, T., 2000. Delayed, disequilibrium degassing in rhyolite magma: decompression experiments and implications for explosive volcanism. Earth and Planetary Science Letters 183 (3), 441–455.
Maret, S., Bergin, E., Lada, C., 2006. A low fraction of nitrogen in molecular form in a dark cloud. Nature 442 (7101), 425–427.
Marion, G., Kargel, J., Catling, D., Lunine, J., 2012. Modeling ammonia-ammonium aqueous chemistries in the solar system's icy bodies. Icarus 220 (2), 932 – 946.
Matson, D. L., Castillo, J. C., Lunine, J., Johnson, T. V., 2007. Enceladus' plume: Compositional evidence for a hot interior. Icarus 187 (2), 569 – 573.
Matson, D. L., Castillo-Rogez, J. C., Davies, A. G., Johnson, T. V., 2012. Enceladus: A hypothesis for bringing both heat and chemicals to the surface. Icarus.
McComas, D., Allegrini, F., Bagenal, F., Casey, P., Delamere, P., Demkee, D., Dunn, G., Elliott, H., Hanley, J., Johnson, K., et al., 2008. The solar wind around pluto (swap) instrument aboard new horizons. Space Science Reviews 140, 261–313.
McKinnon, W. B., 2002. On the initial thermal evolution of Kuiper belt objects. In: Asteroids, Comets, and Meteors: ACM 2002. Vol. 500. pp. 29–38.
McKinnon, W. B., Prialnik, D., Stern, S. A., Coradini, A., 2008. Structure and evolution of Kuiper belt objects and dwarf planets. The Solar System Beyond Neptune 1, 213–241.
McNutt, R. L., Livi, S. A., Gurnee, R. S., Hill, M. E., Cooper, K. A., Andrews, G. B., Keath, E. P., Krimigis, S. M., Mitchell, D. G., Tossman, B., et al., 2008. The pluto energetic particle spectrometer science investigation (pepssi) on the new horizons mission. Space Science Reviews 140 (1-4), 315–385.
Merlin, F., Barucci, M., de Bergh, C., DeMeo, F., Alvarez-Candal, A., Dumas, C., Cruikshank, D., 2010. Chemical and physical properties of the variegated Pluto and Charon surfaces. Icarus 210 (2), 930–943.
Miller, G. A., Carpenter, D. K., 1964. Solid-liquid phase diagram of the system methanol-water. Journal of Chemical & Engineering Data 9 (3), 371–373.
Mironenko, M. V., Boitnott, G. E., Grant, S. A., Sletten, R. S., 2001. Experimental determination of the volumetric properties of NaCl solutions to 253 K. The Journal of Physical Chemistry B 105 (41), 9909–9912.
Mishima, O., 2010. Volume of supercooled water under pressure and the liquid-liquid critical point. The Journal of Chemical Physics 133, 144503.
Mousis, O., Lunine, J., Waite, J., Magee, B., Lewis, W., Mandt, K., Marquer, D., Cordier, D., 2009. Formation conditions of Enceladus and origin of its methane reservoir. The Astrophysical Journal Letters 701 (1), L39.
Mumma, M. J., Charnley, S. B., 2011. The chemical composition of comets - Emerging taxonomies and natal heritage. Astronomy and Astrophysics 49 (1), 471.
Nelson, R. M., Kamp, L. W., Lopes, R. M. C., Matson, D. L., Kirk, R. L., Hapke, B. W., Wall, S. D., Boryta, M. D., Leader, F. E., Smythe, W. D., Mitchell, K. L., Baines, K. H., Jaumann, R., Sotin, C., Clark, R. N., Cruikshank, D. P., Drossart, P., Lunine, J. I., Combes, M., Bellucci, G., Bibring, J.-P., Capaccioni, F., Cerroni, P., Coradini, A., Formisano, V., Filacchione, G., Langevin, Y., McCord, T. B., Mennella, V., Nicholson, P. D., Sicardy, B., Irwin, P. G. J., Pearl, J. C., 2009. Photometric changes on Saturn's Titan: Evidence for active cryovolcanism. Geophysical Research Letters 36 (4), L04202.
Opeil, C., Consolmagno, G., Britt, D., 2010. The thermal conductivity of meteorites: New measurements and analysis. Icarus 208 (1), 449–454.
Pitzer, K. S., 1973. Thermodynamics of electrolytes. I. Theoretical basis and general equations. The Journal of Physical Chemistry 77 (2), 268–277.
Plyasunov, A. V., Shock, E. L., 2001. Correlation strategy for determining the parameters of the revised Helgeson-Kirkham-Flowers model for aqueous nonelectrolytes. Geochimica et Cosmochimica Acta 65 (21), 3879–3900.
Porco, C. C., Helfenstein, P., Thomas, P. C., Ingersoll, A. P., Wisdom, J., West, R., Neukum, G., Denk, T., Wagner, R., Roatsch, T., Kieffer, S., Turtle, E., McEwen, A., Johnson, T. V., Rathbun, J., Veverka, J., Wilson, D., Perry, J., Spitale, J., Brahic, A., Burns, J. A., DelGenio, A. D., Dones, L., Murray, C. D., Squyres, S., 2006. Cassini observes the active south pole of Enceladus. Science 311 (5766), 1393–1401.
Porter, S. B., Desch, S. J., Cook, J. C., 2010. Micrometeorite impact annealing of ice in the outer solar system. Icarus 208 (1), 492–498.
Postberg, F., Kempf, S., Schmidt, J., Brilliantov, N., Beinsen, A., Abel, B., Buck, U., Srama, R., 2009. Sodium salts in E-ring ice grains from an ocean below the surface of Enceladus. Nature 459 (7250), 1098–1101.
Prialnik, D., Sarid, G., Rosenberg, E. D., Merk, R., 2008. Thermal and chemical evolution of comet nuclei and Kuiper belt objects. Space Science Reviews 138 (1-4), 147–164.
Proussevitch, A., Sahagian, D., 1998. Dynamics and energetics of bubble growth in magmas: analytical formulation and numerical modeling. Journal of Geophysical Research: Solid Earth (1978–2012) 103 (B8), 18223–18251.
Reuter, D., Stern, S., Scherrer, J., Jennings, D., Baer, J., Hanley, J., Hardaway,

L., Lunsford, A., McMuldroch, S., Moore, J., Olkin, C., Parizek, R., Reitsma, H., Sabatke, D., Spencer, J., Stone, J., Throop, H., Van Cleve, J., Weigle, G., Young, L., 2008. Ralph: A Visible/Infrared Imager for the New Horizons Pluto/Kuiper Belt Mission. Space Science Reviews 140, 129–154, 10.1007/s11214-008-9375-7.

Robuchon, G., Nimmo, F., 2011. Thermal evolution of Pluto and implications for surface tectonics and a subsurface ocean. Icarus 216 (2), 426 – 439.

Rosner, D. E., Epstein, M., 1972. Effects of interface kinetics, capillarity and solute diffusion on bubble growth rates in highly supersaturated liquids. Chemical Engineering Science 27 (1), 69–88.

Roth, L., Saur, J., Retherford, K. D., Strobel, D. F., Feldman, P. D., McGrath, M. A., Nimmo, F., 2014. Transient water vapor at Europa's south pole. Science Express, 4 pp.

Rousselot, P., Pirali, O., Jehin, E., Vervloet, M., Hutsemékers, D., Manfroid, J., Cordier, D., Martin-Drumel, M.-A., Gruet, S., Arpigny, C., et al., 2014. Toward a unique nitrogen isotopic ratio in cometary ices. The Astrophysical Journal Letters 780 (2), L17.

Rubin, M. E., Neveu, M., Desch, S. J., in review. Effect of Rayleigh-Taylor instabilities on the differentiation of intermediate-sized icy bodies. In review.

Sandford, S. A., Aléon, J., Alexander, C. M., Araki, T., Bajt, S., Baratta, G. A., Borg, J., Bradley, J. P., Brownlee, D. E., Brucato, J. R., et al., 2006. Organics captured from comet 81P/Wild 2 by the Stardust spacecraft. Science 314 (5806), 1720–1724.

Schaller, E. L., Brown, M. E., 2007. Volatile loss and retention on Kuiper belt objects. The Astrophysical Journal Letters 659 (1), L61.

Schenk, P. M., 1991. Fluid volcanism on Miranda and Ariel: Flow morphology and composition. Journal of Geophysical Research: Solid Earth (1978–2012) 96 (B2), 1887–1906.

Schmidt, B., Blankenship, D., Patterson, G., Schenk, P., 2011. Active formation of chaos terrain over shallow subsurface water on europa. Nature 479 (7374), 502–505.

Schulte, M. D., Shock, E. L., 1993. Aldehydes in hydrothermal solution: Standard partial molal thermodynamic properties and relative stabilities at high temperatures and pressures. Geochimica et Cosmochimica Acta 57 (16), 3835–3846.

Shock, E. L., 1993. Hydrothermal dehydration of aqueous organic compounds. Geochimica et Cosmochimica Acta 57 (14), 3341–3349.

Shock, E. L., 1995. Organic acids in hydrothermal solutions: standard molal thermodynamic properties of carboxylic acids and estimates of dissociation constants at high temperatures and pressures. American Journal of Science 295 (5), 496.

Shock, E. L., Helgeson, H. C., 1988. Calculation of the thermodynamic and transport properties of aqueous species at high pressures and temperatures: Correlation algorithms for ionic species and equation of state predictions to 5 kb and 1000°C. Geochimica et Cosmochimica Acta 52 (8), 2009–2036.

Shock, E. L., Helgeson, H. C., Sverjensky, D. A., 1989. Calculation of the thermodynamic and transport properties of aqueous species at high pressures and temperatures: Standard partial molal properties of inorganic neutral species. Geochimica et Cosmochimica Acta 53 (9), 2157–2183.

Shock, E. L., McKinnon, W. B., 1993. Hydrothermal processing of cometary volatiles: Applications to Triton. Icarus 106 (2), 464–477.

Sicardy, B., Widemann, T., Lellouch, E., Veillet, C., Cuillandre, J.-C., Colas, F., Roques, F., Beisker, W., Kretlow, M., Lagrange, A.-M., Gendron, E., Lacombe, F., Lecacheux, J., Birnbaum, C., Fienga, A., Leyrat, C., Maury, A., Raynaud, E., Renner, S., Schultheis, M., Brooks, K., Delsanti, A., Hainaut, O. R., Gilmozzi, R., Lidman, C., Spyromilio, J., Rapaport, M., Rosenzweig, P., Naranjo, O., Porras, L., Diaz, F., Calderon, H., Carrillo, S., Carvajal, A., Recalde, E., Cavero, L. G., Montalvo, C., Barria, D., Campos, R., Duffard, R., Levato, H., 2003. Large changes in Pluto's atmosphere as revealed by recent stellar occultations. Nature 424 (6945), 168–170.

Smith, B. A., Soderblom, L. A., Banfield, D., Barnet, C., Basilevsky, A. T., Beebe, R. F., Bollinger, K., Boyce, J. M., Brahic, A., Briggs, G. A., Brown, R. H., Chyba, C., Collins, S. A., Colvin, T., Cook, A. F., Crisp, D., Croft, S. K., Cruikshank, D., Cuzzi, J. N., Danielson, G. E., Davies, M. E., De Jong, E., Dones, L., Godfrey, D., Goguen, J., Grenier, I., Haemmerle, V. R., Hammel, H., Hansen, C. J., Helfenstein, c. P., Howell, C., Hunt, G. E., Ingersoll, A. P., Johnson, T. V., Kargel, J., Kirk, R., Kuehn, D. I., Limaye, S., Masursky, H., McEwen, A., Morrison, D., Owen, T., Owen, W., Pollack, J. B., Porco, C. C., Rages, K., Rogers, P., Rudy, D., Sagan, C., Schwartz, J., Shoemaker, E. M., Showalter, M., Sicardy, B., Simonelli, D., Spencer, J., Sromovsky, L. A., Stoker, C., Strom, R. G., Suomi, V. E., Synott, S. P., Terrile, R. J., Thomas, P., Thompson, W. R., Verbiscer, A., Veverka, J., 1989. Voyager 2 at Neptune: Imaging science results. Science 246 (4936), 1422–1449.

Soderblom, L., Kieffer, S., Becker, T., Brown, R., Cook, A., Hansen, C., Johnson, T., Kirk, R., Shoemaker, E., 1990. Triton's geyser-like plumes: Discovery and basic characterization. Science 250 (4979), 410–415.

Soderblom, L. A., Brown, R. H., Soderblom, J. M., Barnes, J. W., Kirk, R. L., Sotin, C., Jaumann, R., Mackinnon, D. J., Mackowski, D. W., Baines, K. H., Buratti, B. J., Clark, R. N., Nicholson, P. D., 2009. The geology of Hotei Regio, Titan: correlation of Cassini VIMS and RADAR. Icarus 204 (2), 610–618.

Sotin, C., Jaumann, R., Buratti, B. J., Brown, R. H., Clark, R. N., Soderblom, L. A., Baines, K. H., Bellucci, G., Bibring, J.-P., Capaccioni, F., Cerroni, P., Combes, M., Coradini, A., Cruikshank, D. P., Drossart, P., Formisano, V., Langevin, Y., Matson, D. L., McCord, T. B., Nelson, R. M., Nicholson, P. D., Sicardy, B., LeMouelic, S., Rodriguez, S., Stephan, K., Scholz, C. K., 2005. Release of volatiles from a possible cryovolcano from near-infrared imaging of Titan. Nature 435 (7043), 786–789.

Sparks, R., 1978. The dynamics of bubble formation and growth in magmas: a review and analysis. Journal of Volcanology and Geothermal Research 3 (1), 1–37.

Speedy, R., Angell, C., 1976. Isothermal compressibility of supercooled water and evidence for a thermodynamic singularity at −45°C. The Journal of Chemical Physics 65 (3), 851.

Stern, A., Spencer, J., 2003. New horizons: The first reconnaissance mission to bodies in the kuiper belt. Earth, Moon, and Planets 92 (1-4), 477–482.

Stern, S., Slater, D., Festou, M., Parker, J. W., Gladstone, G., AHearn, M., Wilkinson, E., 2000. The discovery of argon in comet C/1995 O1 (Hale-Bopp). The Astrophysical Journal Letters 544 (2), L169.

Stern, S. A., Slater, D. C., Scherrer, J., Stone, J., Dirks, G., Versteeg, M., Davis, M., Gladstone, G. R., Parker, J. W., Young, L. A., et al., 2008. Alice: The ultraviolet imaging spectrograph aboard the new horizons pluto–kuiper belt mission. Space Science Reviews 140 (1-4), 155–187.

Stevenson, D., 1982. Volcanism and igneous processes in small icy satellites. Nature 298, 142–144.

Thomas, P. J., Reynolds, R. T., Squyres, S. W., Cassen, P. M., 1987. The viscosity of Miranda. In: Lunar and Planetary Institute Science Conference Abstracts. Vol. 18 of Lunar and Planetary Institute Science Conference Abstracts. p. 1016.

Tobie, G., Lunine, J. I., Sotin, C., 2006. Episodic outgassing as the origin of atmospheric methane on Titan. Nature 440 (7080), 61–64.

Tromans, D., Meech, J., 2002. Fracture toughness and surface energies of minerals: theoretical estimates for oxides, sulphides, silicates and halides. Minerals engineering 15 (12), 1027–1041.

Trump, J. E. V., Miller, S. L., 1973. Carbon monoxide on the primitive Earth. Earth and Planetary Science Letters 20, 145–150.

Tyler, G., Linscott, I., Bird, M., Hinson, D., Strobel, D., Pätzold, M., Summers, M., Sivaramakrishnan, K., 2008. The new horizons radio science experiment (rex). Space science reviews 140 (1-4), 217–259.

Wagman, D. D., Evans, W. H., Parker, V. B., Schumm, R. H., Halow, I., 1982. The NBS tables of chemical thermodynamic properties. Selected values for inorganic and C1 and C2 organic substances in SI units. Tech. rep., DTIC Document.

Wagner, W., Pruss, A., 2002. The IAPWS formulation 1995 for the thermodynamic properties of ordinary water substance for general and scientific use. Journal of Physical and Chemical Reference Data 31 (2), 387–536.

Waite Jr, J. H., Lewis, W. S., Magee, B. A., Lunine, J. I., McKinnon, W. B., Glein, C. R., Mousis, O., Young, D. T., Brockwell, T., Westlake, J., Nguyen, M.-J., Teolis, B. D., Niemann, H. B., McNutt Jr, R. L., Perry, M., Ip, W.-H., 2009. Liquid water on Enceladus from observations of ammonia and 40Ar in the plume. Nature 460 (7254), 487–490.

Wall, S. D., Lopes, R. M., Stofan, E. R., Wood, C. A., Radebaugh, J. L., Hrst, S. M., Stiles, B. W., Nelson, R. M., Kamp, L. W., Janssen, M. A., Lorenz, R. D., Lunine, J. I., Farr, T. G., Mitri, G., Paillou, P., Paganelli, F., Mitchell, K. L., 2009. Cassini RADAR images at Hotei Arcus and western Xanadu, Titan: Evidence for geologically recent cryovolcanic activity. Geophysical Research Letters 36 (4), L04203.

Wang, J.-J., Zhu, J.-G., Chiu, C., Zhang, H., 2007. Experimental study on fracture toughness and tensile strength of a clay. Engineering Geology 94 (1), 65–75.

Yomogida, K., Matsui, T., 1983. Physical properties of ordinary chondrites.

Journal of Geophysical Research 88 (B11), 9513–9533.
Young, P. A., Desch, S. J., Anbar, A. D., Barnes, R., Hinkel, N. R., Kopparappu, R., Madhusudhan, N., Monga, N., Pagano, M. D., Riner, M. A., Scannapieco, E., Shim, S.-H., Truitt, A., 2014. Stellar stoichiometry. Astrobiology, in press.
Yund, R. A., McCallister, R. H., 1970. Kinetics and mechanisms of exsolution. Chemical Geology 6, 5–30.
Zhong, F., Mitchell, K. L., Hays, C. C., Choukroun, M., Barmatz, M., Kargel, J. S., 2009. The rheology of cryovolcanic slurries: motivation and phenomenology of methanol-water slurries with implications for Titan. Icarus 202 (2), 607–619.
Zolotov, M. Y., 2012. Aqueous fluid composition in CI chondritic materials: Chemical equilibrium assessments in closed systems. Icarus 220, 713–729.

Appendix A. Implementation of the geochemical model

Equation (6) translates into:

$$m_i M_{\rm liq} + \frac{P_i x_{\rm vap} M_{\rm liq}}{\rho_{\rm liq} RT} = A_{i,w} \tag{A.1}$$

where all terms are abundances in mol. $M_{\rm liq} = \rho_{\rm liq} V_{\rm liq}$ is the total mass of liquid in the body and $x_{\rm vap} = V_{\rm gas}/V_{\rm liq}$ is the overall volumic vapor fraction. Using equation (5), this becomes:

$$m_i M_{\rm liq} \left(1 + \frac{x_{\rm vap}}{K_i \rho_{\rm liq} RT}\right) = A_{i,w} \tag{A.2}$$

Equivalently:

$$P_i = \frac{A_{i,w}}{K_i M_{\rm liq} \left(1 + \frac{x_{\rm vap}}{K_i \rho_{\rm liq} RT}\right)} \tag{A.3}$$

Therefore, equation (7) becomes:

$$\sum_{i=1}^{n_{\rm species}} \frac{A_{i,w}}{M_{\rm liq} \left(K_i + \frac{x_{\rm vap}}{\rho_{\rm liq} RT}\right)} = P_{\rm gas} \tag{A.4}$$

where P is the local pressure. Solving equation (A.4) requires finding the root of a polynomial of degree $n_{\rm species}$ in $X = x_{\rm vap}/(\rho_{\rm liq} RT)$,

$$P_{\rm gas} M_{\rm liq} \prod_{i=1}^{n_{\rm species}} (K_i + X) - \sum_{i=1}^{n_{\rm species}} A_{i,w} \prod_{\substack{j=1 \\ j \neq i}}^{n_{\rm species}} (K_j + X) = 0 \tag{A.5}$$

The variable X has same units as K_i: mol kg^{-1} bar^{-1} in our assumption of negligible salinity. In principle, this polynomial has $n_{\rm species}$ complex roots. In practice, the coefficients in front of the positive terms ($P_{\rm gas} M_{\rm liq} \approx 10^{26}$ Pa kg), whose largest degree is $n_{\rm species}$, are much larger than those in front of the negative terms ($A_{i,w} \approx 10^{18}$ mol), whose largest degree is only $n_{\rm species} - 1$. This causes the polynomial to increase monotonically in the range of physically plausible X ($X > 0$), except at small X ($X \ll \min[K_i]$). When X is very small, the K_i terms dominate X. The sum term with the largest $K_i \approx 10^3$ (here taken as a dimensionless equilibrium constant) likely dominates the polynomial if its $A_{i,w}$ is not exceptionally low, since the product of all K_i is only about 10^{-8} for the ten species accounted for in this paper. At $P_{\rm gas}$ less or equal than a typical value at the seafloor of dwarf planets (30 MPa), this is enough for the polynomial to become negative at small X, which guarantees that equation (A.5) has a single real positive root. (At higher $P \gtrsim 150$ MPa with our choice of species and bulk abundances, the polynomial is positive for all $X > 0$ and only has negative roots: physically, exsolution does not occur.) This root was found using a combined bisection/Newton-Raphson algorithm.

Knowing X, the molalities and partial pressures of all species are obtained from equation (A.2):

$$m_i = \frac{A_{i,w}/M_{\rm liq}}{1 + X/K_i} \tag{A.6}$$

$$P_i = m_i / K_i \tag{A.7}$$

Throughout the algorithm, one needs to pay special attention to the pressure units, because P_i are in bar in equation (5), but in Pa in equations (6) and (7).